Electronic Supplementary Information

Something germane about germanium: facile access to Ge_{10} adamantane

Sebastian Karger, Elias Drösemeier, Alexander V. Virovets, Eugenia Peresypkina
Hans-Wolfram Lerner, Thomas Müller*, and Matthias Wagner*

Table of contents

1. Experimental Details and Characterization Data

1.1 General Considerations

All reactions were carried out under an inert-gas atmosphere (dry argon or nitrogen) using standard Schlenk or glove-box techniques. *n*-Pentane, *n*-hexane, and THF were dried over Na metal; toluene was dried over Na/benzophenone. All solvents were distilled prior to use and stored over molecular sieves (3 Å). C_6D_6 was stored over molecular sieves (3 Å). THF-d_8 was dried over Na-K alloy, distilled prior to use, and stored over molecular sieves (3 Å). KO*t*Bu, Me_3GeCl, 18-crown-6, and $[Ph_3C][B(C_6F_5)_4]$ were purchased and used as received. $\mathbf{B^{TMS}}$ was prepared according to published procedures.[S1] During the course of this work, the reaction was scaled up to afford up to 220 mg of $\mathbf{B^{TMS}}$.

NMR spectra were recorded at 298 K on a *Bruker Avance III HD 500* spectrometer equipped with a *Prodigy BBO 500 S1* probe. Chemical shift values are reported in ppm. ^1H and $^{13}C\{^1H\}$ NMR spectra were calibrated to (residual) solvent signals (C_6D_6: 7.16 ppm/128.06 ppm; THF-d_8: 3.58, 1.72 ppm/67.21, 25.31 ppm; s = singlet).[S2] ^{29}Si NMR spectra were calibrated against external $SiMe_4$ ($\delta(^{29}Si)$ = 0). Resonance assignments were supported by two-dimensional $^1H/^{13}C$ HSQC and $^1H/^{29}Si$ HMBC experiments.

High-resolution mass spectra were recorded using a *Thermo Scientific Orbitrap Exploris 240*. UV/vis absorption spectra were recorded at room temperature using a *Varian Cary 60 Scan* UV/vis spectrophotometer. Melting points were measured on an *OptiMelt MPA 100* instrument from *Stanford Research Systems*.

1.2 Synthesis of 1

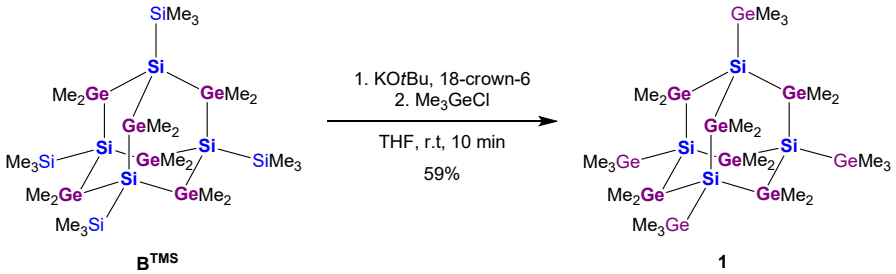

B^{TMS} 1

A solution of Me_3GeCl (0.18 mL, 0.22 g, 1.5 mmol) in THF (1.8 mL) was added dropwise over 10 min to a vigorously stirred solution of $\mathbf{B^{TMS}}$ (185 mg, 0.181 mmol), KO*t*Bu (121 mg, 1.08 mmol), and 18-crown-6 (287 mg, 1.09 mmol) in THF (20 mL). After complete addition, the reaction mixture was stirred for an additional 10 min. All volatiles were removed under reduced pressure, and the colorless residue was extracted into *n*-hexane (3 × 10 mL). All volatiles were removed from the combined extracts under reduced pressure to afford a colorless solid, which was further purified by filtration through silica gel (eluent: *n*-hexane) to furnish **1** as colorless solid. Yield: 0.127 g (0.106 mmol, 59%)

Crystals of **1**·0.75(C_5H_{12}) suitable for X-ray crystal structure analysis were grown by slow evaporation of an *n*-pentane solution.

^{1}H NMR (500.2 MHz, C_6D_6): δ = 0.72 (s, 36H, $GeMe_2$), 0.46 (s, 36H, $GeMe_3$).

^{13}C{^{1}H} NMR (125.8 MHz, C_6D_6): δ = 3.8 ($GeMe_3$), 3.7 ($GeMe_2$).

^{29}Si DEPT-6P NMR (99.4 MHz, C_6D_6): δ = −88.8 (Si–$GeMe_3$).

HRMS (ESI): *m/z* calculated for $C_{24}H_{73}Ge_{10}Si_4$ $[M+H]^+$: 1212.6907; found: 1212.6910.

UV/vis (C_6H_{12}): see Table S1 and Figure S16.

Melting point: > 250 °C (decomposition)

Note: The synthesis of **1** was also attempted using the formally required stoichiometry of 1 $\mathbf{B^{TMS}}$: 4 KO*t*Bu : 4 18-crown-6 : 4 Me_3GeCl. To a solution of $\mathbf{B^{TMS}}$ (15.0 mg, 0.0147 mmol), KO*t*Bu (6.6 mg, 0.059 mmol), and 18-crown-6 (15.5 mg, 0.0586 mmol) in THF (3 mL), a solution of Me_3GeCl (0.0073 mL, 0.0091 g, 0.059 mmol) in THF (0.5 mL) was added dropwise at room temperature. The reaction mixture was stirred for 10 min. All volatiles were removed under reduced pressure. ^{1}H and ^{29}Si NMR spectroscopy revealed only an unselective reaction.

1.3 Plots of NMR Spectra (^{1}H,^{29}Si DEPT-6P, $^{1}H/^{29}Si$ HMBC, $^{13}C\{^{1}H\}$, $^{1}H/^{13}C$ HSQC) of 1

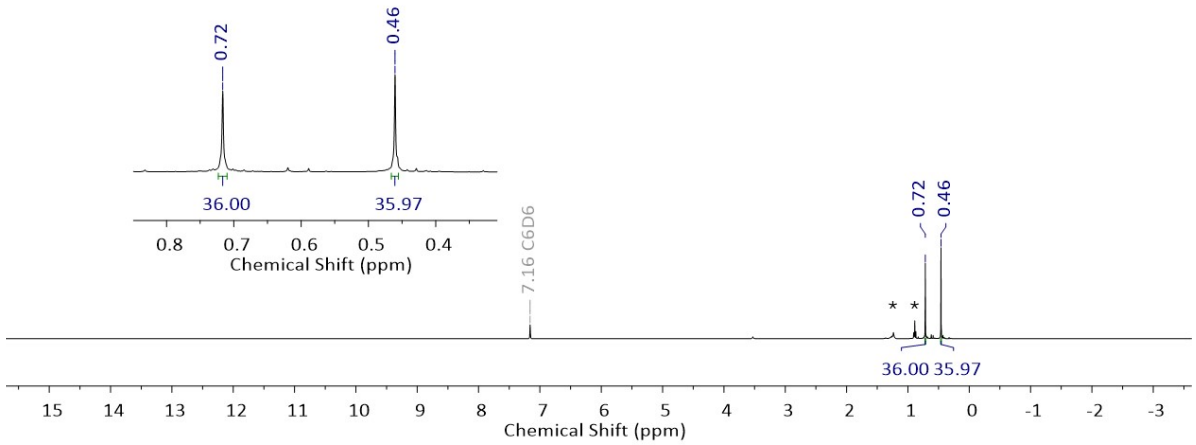

Figure S1. ^{1}H NMR spectrum of **1** (500.2 MHz, C_6D_6). Signals of residual *n*-hexane are marked with asterisks.

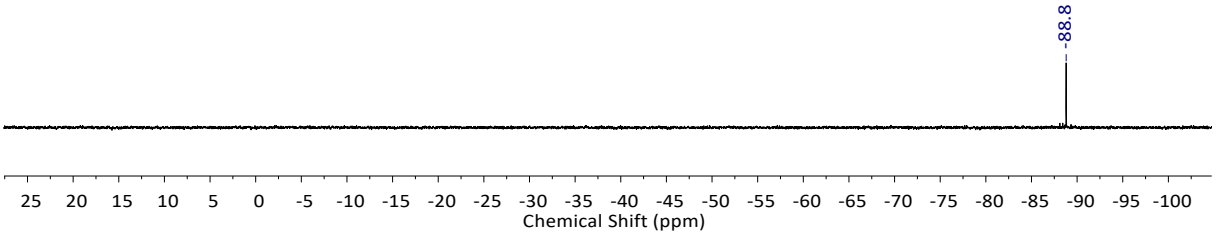

Figure S2. ^{29}Si DEPT-6P NMR spectrum of **1** (99.4 MHz, C_6D_6).

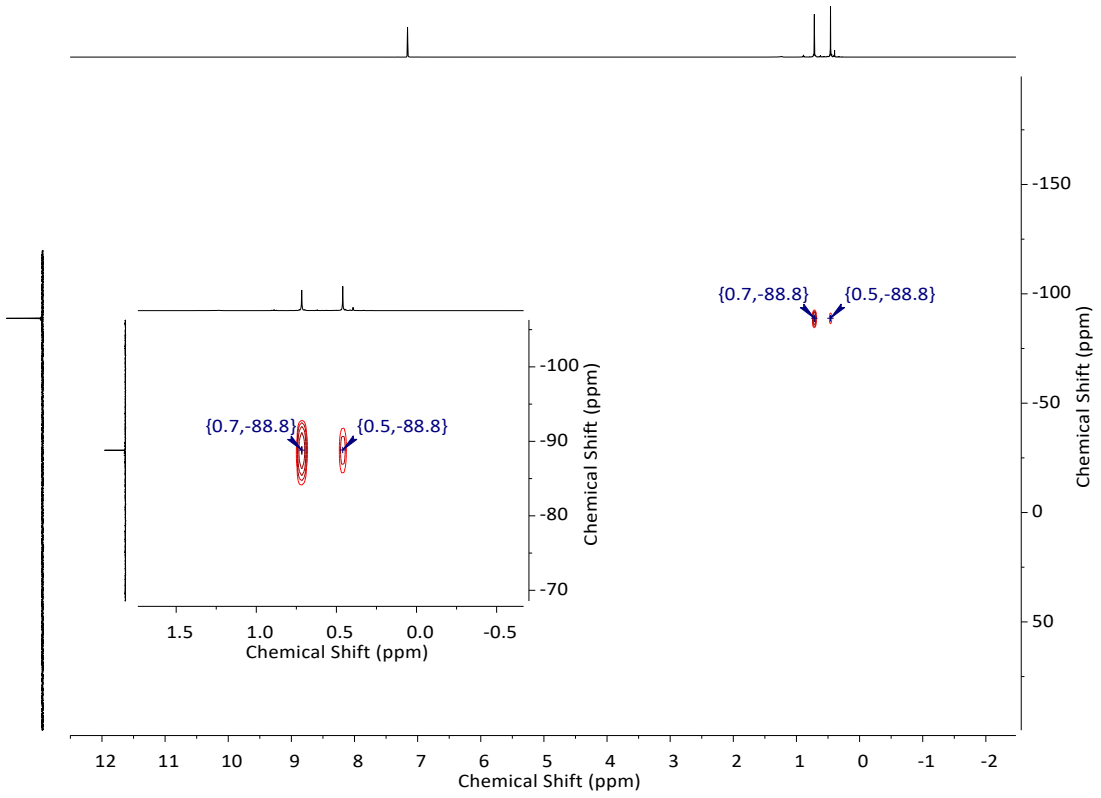

Figure S3. $^{1}H/^{29}Si$ HMBC NMR spectrum of compound **1** (500.2/99.4 MHz, C_6D_6).

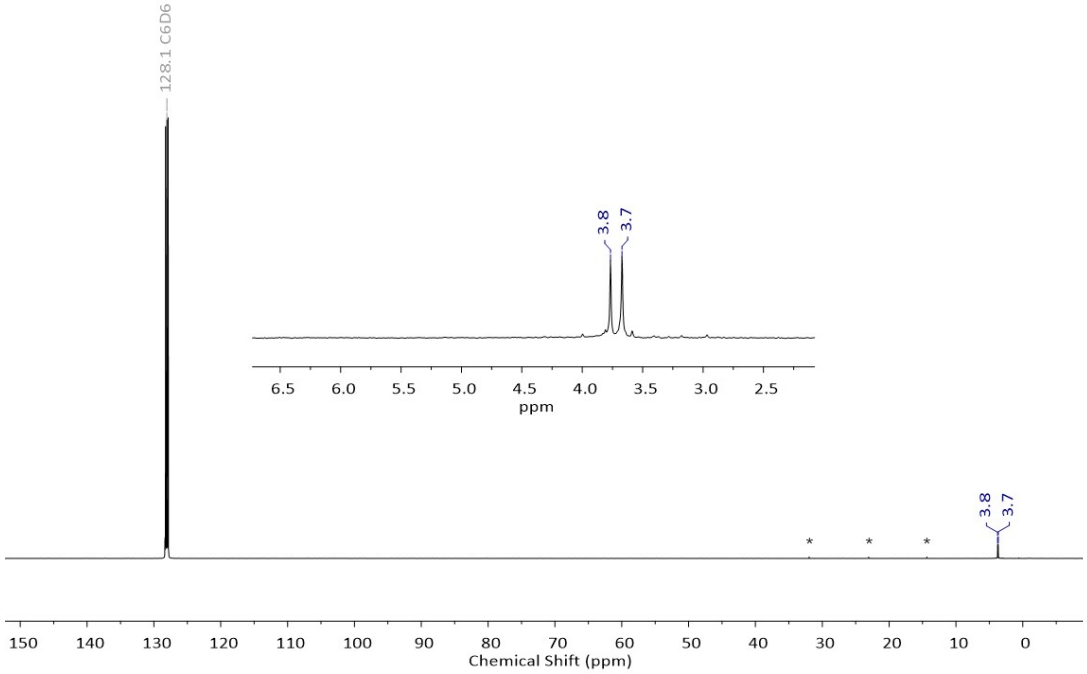

Figure S4. $^{13}C\{^{1}H\}$ NMR spectrum of **1** (125.8 MHz, C_6D_6). Signals of residual *n*-hexane are marked with asterisks.

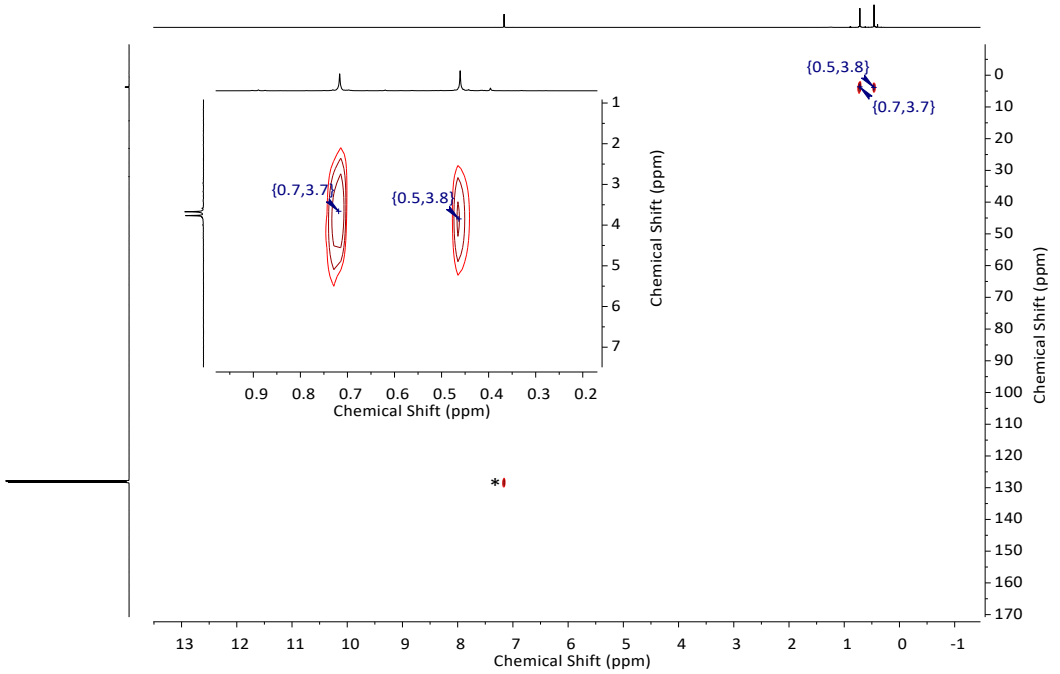

Figure S5. $^{1}H/^{13}C$ HSQC NMR spectrum of compound **1** (500.2/125.8 MHz, C_6D_6). The signal of C_6D_6 is marked with an asterisk.

1.4 Synthesis of 2

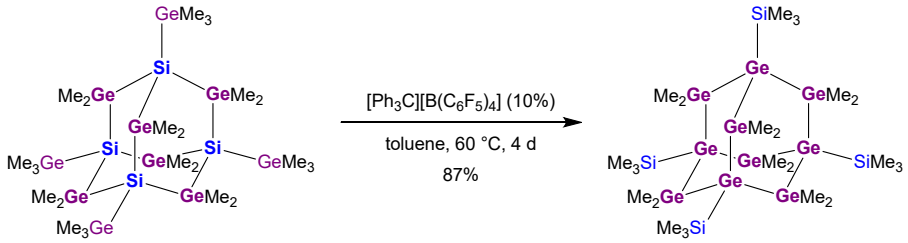

1 **2**

A glass ampoule was charged with a solution of **1** (152 mg, 0.127 mmol) in toluene (5 mL). $[Ph_3C][B(C_6F_5)_4]$ (12 mg, 0.013 mmol) was added, and the ampoule was flame-sealed under vacuum and heated at 60 °C for 4 d. After opening the ampoule, the reaction solution was transferred to a Schlenk flask. All volatiles were removed under reduced pressure, and the brownish residue was extracted into *n*-hexane (3 × 5 mL). All volatiles were removed from the combined extracts under reduced pressure to afford **2** as colorless solid, which was further purified by recrystallization from *n*-hexane. Yield: 132 mg (0.110 mmol, 87%).

Crystals of **2**·0.75(C_5H_{12}) suitable for X-ray crystal structure analysis were grown by slow evaporation of an *n*-pentane solution.

^{1}H NMR (500.2 MHz, C_6D_6): δ = 0.82 (s, 36H, $GeMe_2$), 0.36 (s, 36H, $SiMe_3$).

^{13}C{^{1}H} NMR (125.8 MHz, C_6D_6): δ = 5.7 ($GeMe_2$), 4.8 ($SiMe_3$).

^{29}Si{^{1}H} NMR (99.4 MHz, C_6D_6): δ = 1.4 (Ge–$SiMe_3$).

HRMS (ESI): *m/z* calculated for $C_{24}H_{73}Ge_{10}Si_4$ $[M+H]^+$: 1212.6907; found: 1212.6907.

UV/vis (C_6H_{12}): see Table S1 and Figure S17.

Melting point: > 210 °C (decomposition)

Note: Decomposition of **2** can be observed, upon exposure to air and moisture.

1.5 Plots of NMR Spectra (^{1}H,^{29}Si DEPT-6P, $^{1}H/^{29}Si$ HMBC, $^{13}C\{^{1}H\}$,$^{1}H/^{13}C$ HSQC) of 2

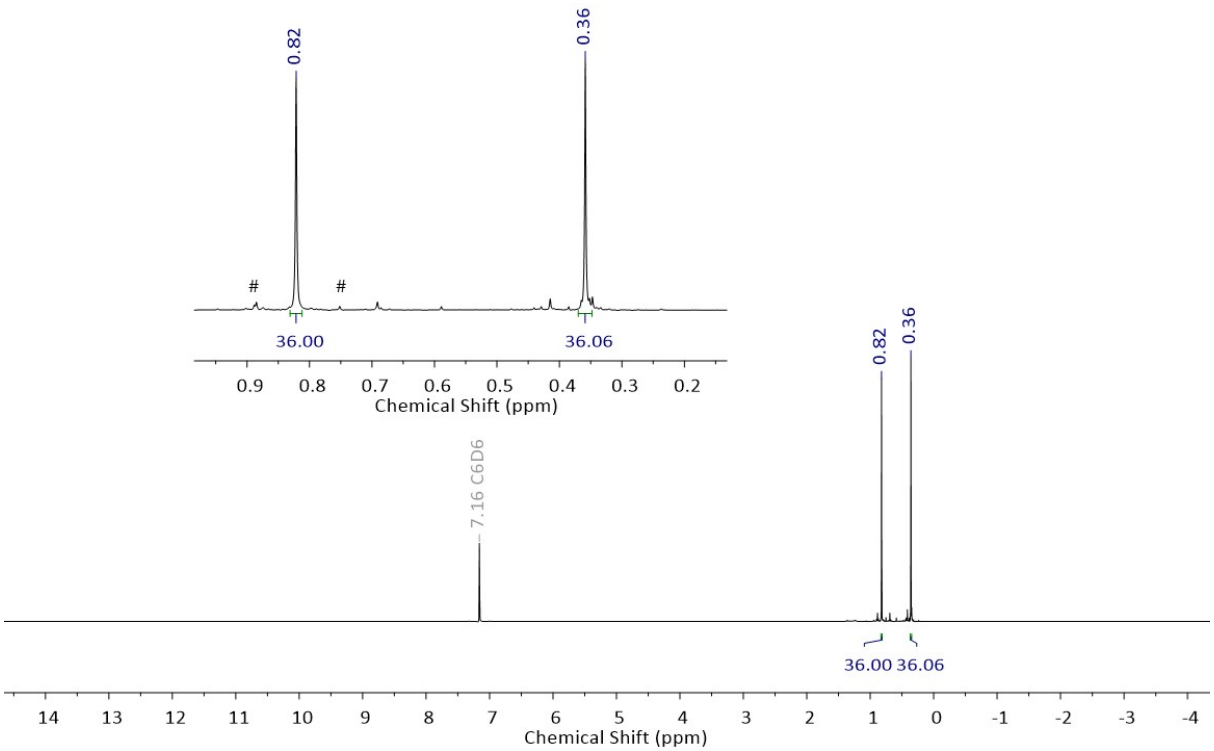

Figure S6. ^{1}H NMR spectrum of **2** (500.2 MHz, C_6D_6). Visible ^{13}C satellites are marked with hash signs.

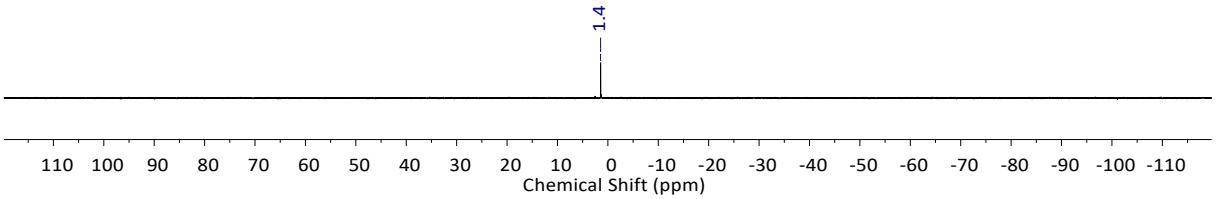

Figure S7. ^{29}Si DEPT-6P NMR spectrum of **2** (99.4 MHz, C_6D_6).

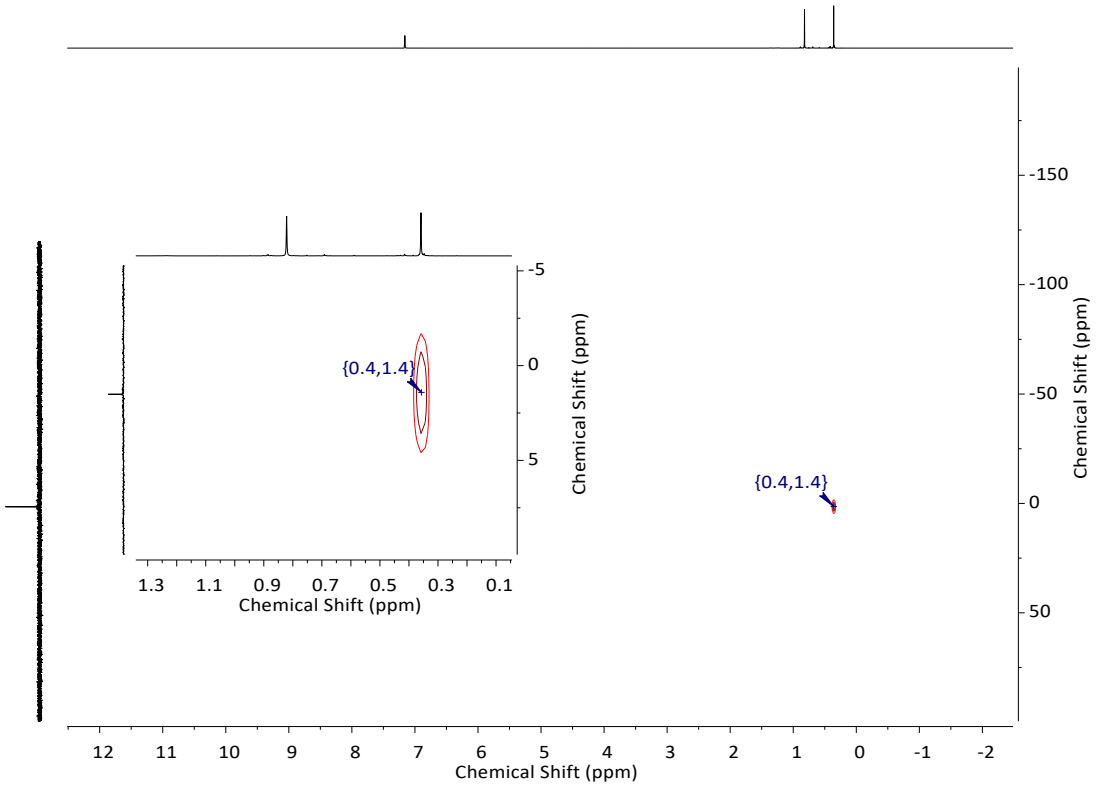

Figure S8. $^{1}H/^{29}Si$ HMBC NMR spectrum of compound **2** (500.2/99.4 MHz, C_6D_6).

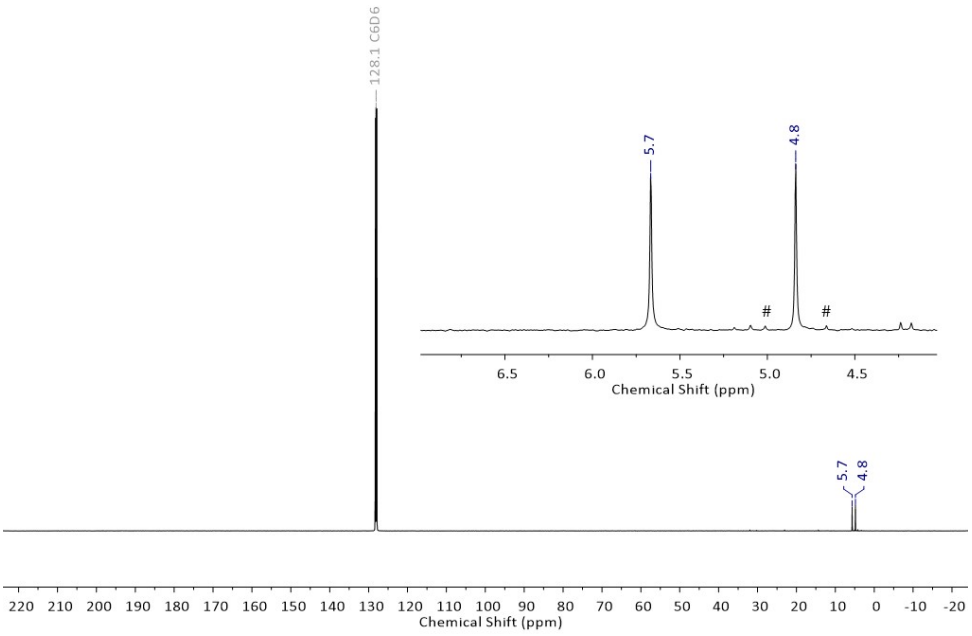

Figure S9. $^{13}C\{^{1}H\}$ NMR spectrum of **2** (125.8 MHz, C_6D_6). ^{29}Si-satellites are marked with hash signs.

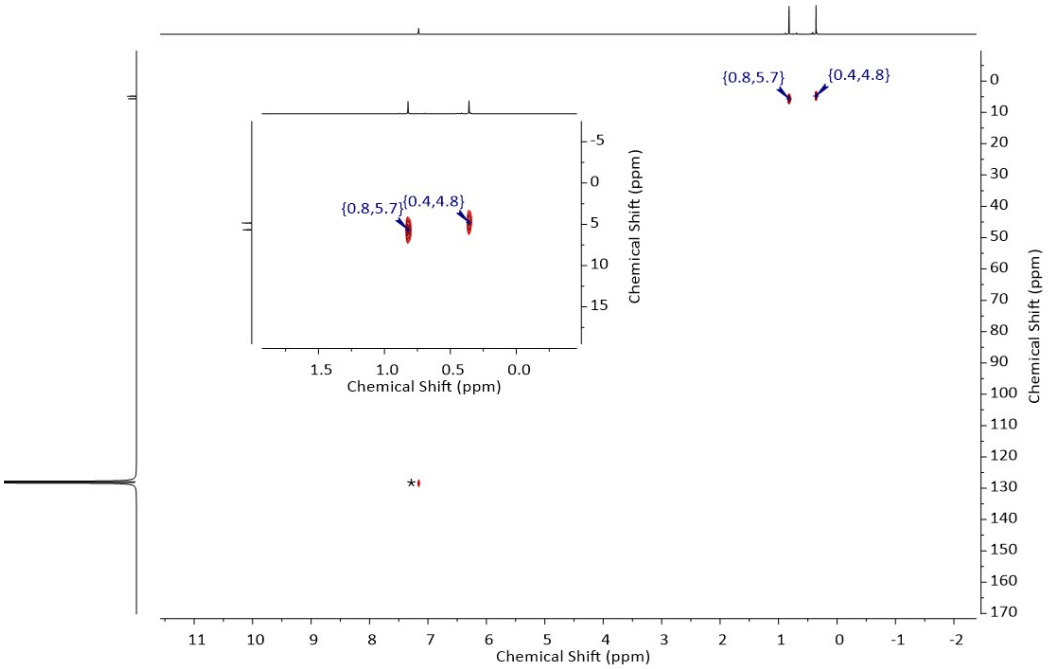

Figure S10. $^{1}H/^{13}C$ HSQC NMR spectrum of compound **2** (500.2/125.8 MHz, C_6D_6). The signal of C_6D_6 is marked with an asterisk.

1.6 Synthesis of [3]$^-$

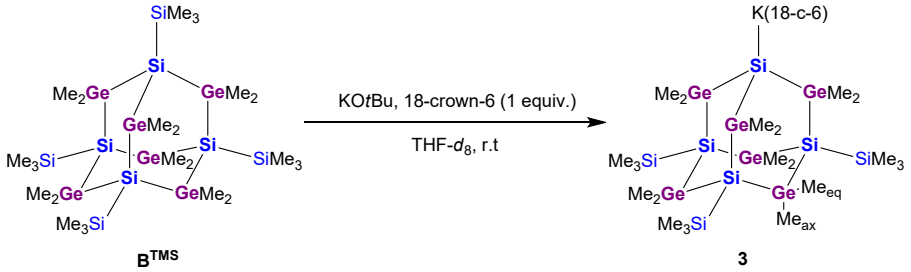

B^{TMS} 3

An NMR-tube was charged with $\mathbf{B^{TMS}}$ (8.0 mg, 0.0078 mmol), KO*t*Bu (0.9 mg, 0.008 mmol), 18-crown-6 (2.2 mg, 0.0083 mmol), and THF-d_8 (0.5 mL) and flame-sealed under reduced pressure. ^{1}H NMR, ^{29}Si DEPT-6P NMR, and ^{1}H/^{29}Si HMBC spectroscopy revealed the immediate formation of [**3**]$^-$.

Crystals of [K(18-c-6)][**3**] suitable for X-ray crystal structure analysis were grown from a saturated C_6H_6 solution.

^{1}H NMR (500.2 MHz, THF-d_8): δ = 0.52 (s, 9H, $GeMe_{ax}$ or $GeMe_{eq}$) 0.51 (s, 9H, $GeMe_{ax}$ or $GeMe_{eq}$), 0.35 (s, 18H, $GeMe_2$), 0.21 (s, 27H, $SiMe_3$).

^{13}C{^{1}H} NMR (125.8 MHz, THF-d_8): δ = 6.9 ($GeMe_2$), 5.7 ($GeMe_{ax}$ or $GeMe_{eq}$), 5.5 ($SiMe_3$), 4.5 ($GeMe_{ax}$ or $GeMe_{eq}$).

^{29}Si DEPT-6P NMR (99.4 MHz, THF-d_8): δ = –5.1 ($SiMe_3$), –96.3 (Si^-), –109.4 (*Si*–$SiMe_3$).

1.7 Plots of NMR Spectra (^{1}H,^{29}Si DEPT-6P, ^{1}H/^{29}Si HMBC, ^{13}C{^{1}H},^{1}H/^{13}C HSQC) of [K(18-c-6)][3]

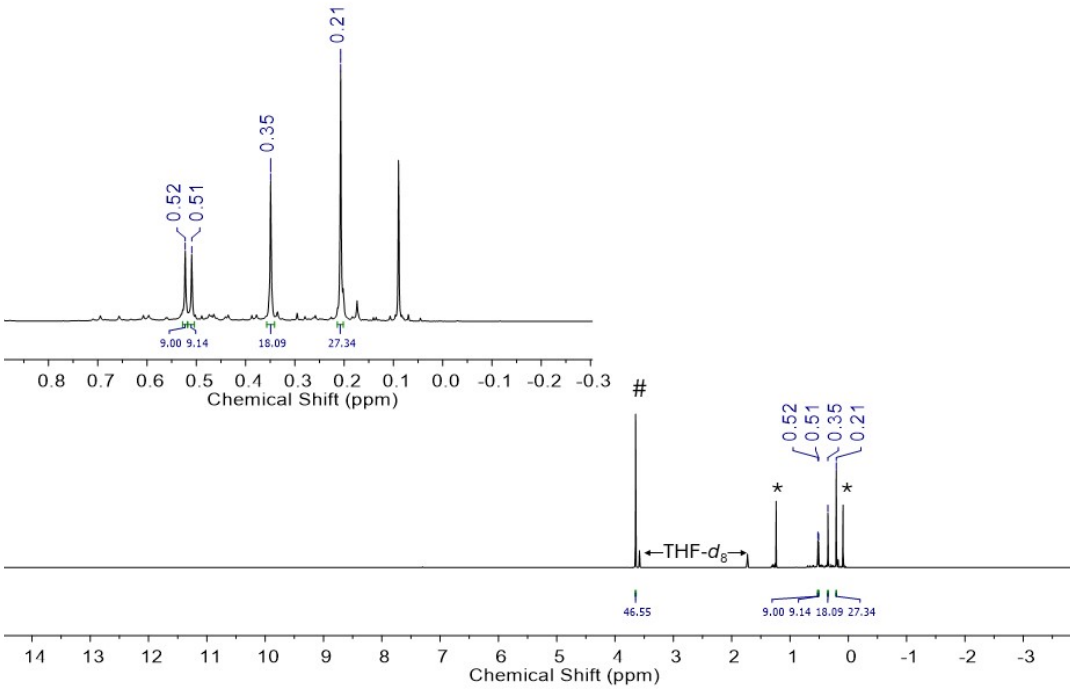

Figure S11. ^{1}H NMR spectrum of [K(18-c-6)][**3**] (500.2 MHz, THF-d_8). 18-crown-6 is marked with a hash sign. Signals for Me_3SiO*t*Bu are marked with asterisks.

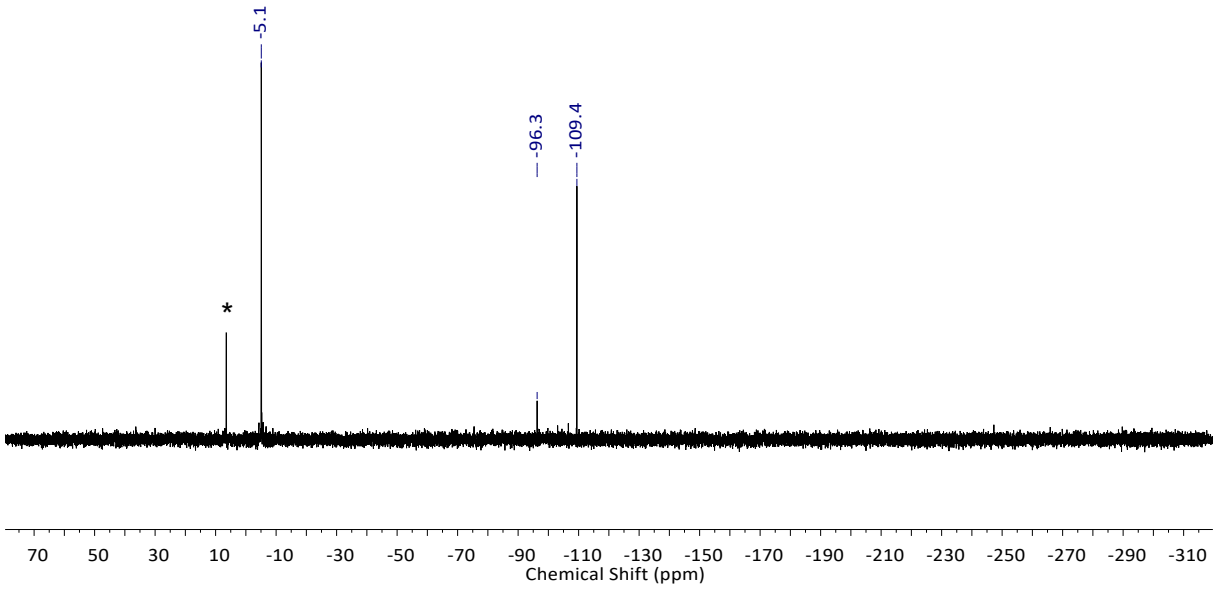

Figure S12. ^{29}Si DEPT-6P NMR spectrum of [K(18-c-6)][**3**] (99.4 MHz, THF-d_8). The signal of Me_3SiO*t*Bu is marked with an asterisk.

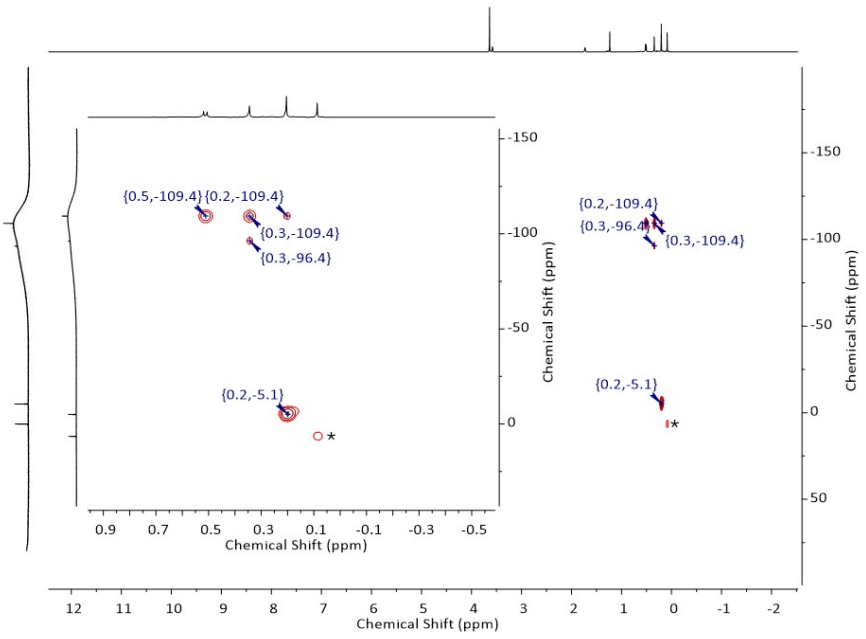

Figure S13. $^{1}H/^{29}Si$ HMBC NMR spectrum of [K(18-c-6)][**3**] (500.2/99.4 MHz, THF-d_8). The signal of $Me_3SiOtBu$ is marked with an asterisk.

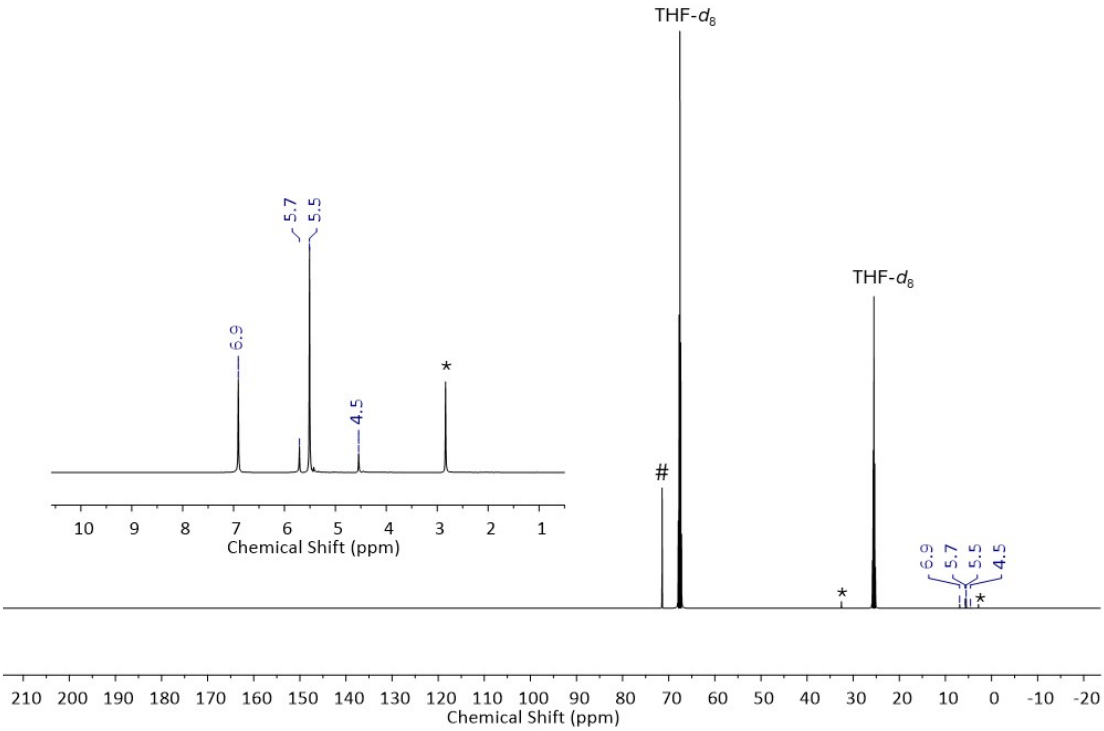

Figure S14. $^{13}C\{^{1}H\}$ NMR spectrum of [K(18-c-6)][**3**] (125.8 MHz, THF-d_8). 18-crown-6 is marked with a hash sign. Signals of $Me_3SiOtBu$ are marked with asterisks.

1.8 UV/vis absorption

Table S1. Photophysical data of the compounds $\mathbf{B^{TMS}}$, **1**, and **2**. Measurements were performed in cyclohexane.

	λ_{max} [nm] (ε [dm^{3}mol^{-1}cm^{-1}])	λ_{onset} [nm][a]	E_G^{opt} [eV][b]
$\mathbf{B^{TMS}}$	226 (1.1 × 10^5)	256	4.84
1	228 (1.1 × 10^5)	258	4.81
2	226 (0.95 × 10^5)	263	4.71

[a] Onset wavelengths (λ_{onset}) were determined by constructing a tangent at the inflection point of the bathochromic slope of the most red-shifted absorption maximum. [b] Optical band gap E_G^{opt} = (1240 eV·nm)/l_{onset}.

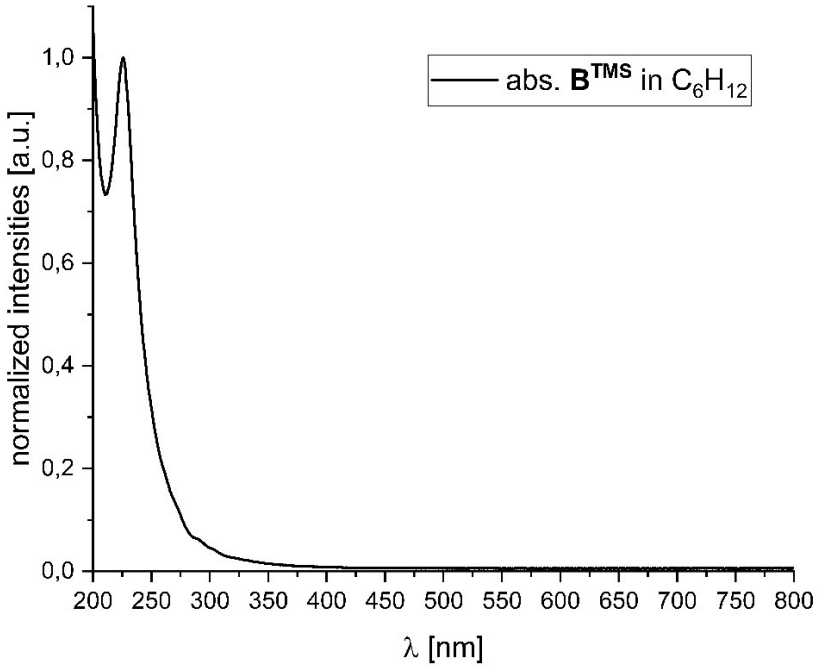

Figure S15. Normalized UV/vis absorption spectrum of $\mathbf{B^{TMS}}$ in cyclohexane.

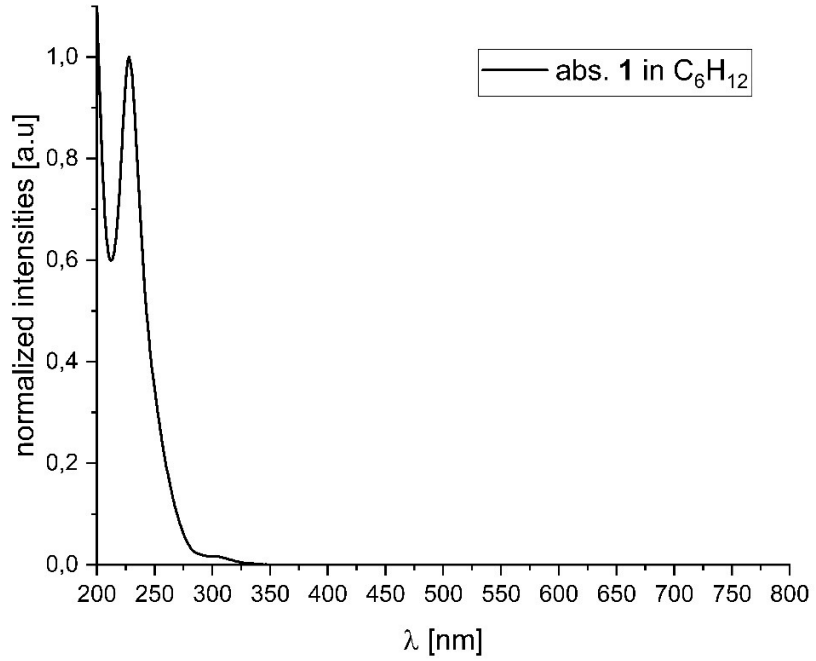

Figure S16. Normalized UV/vis absorption spectrum of **1** in cyclohexane.

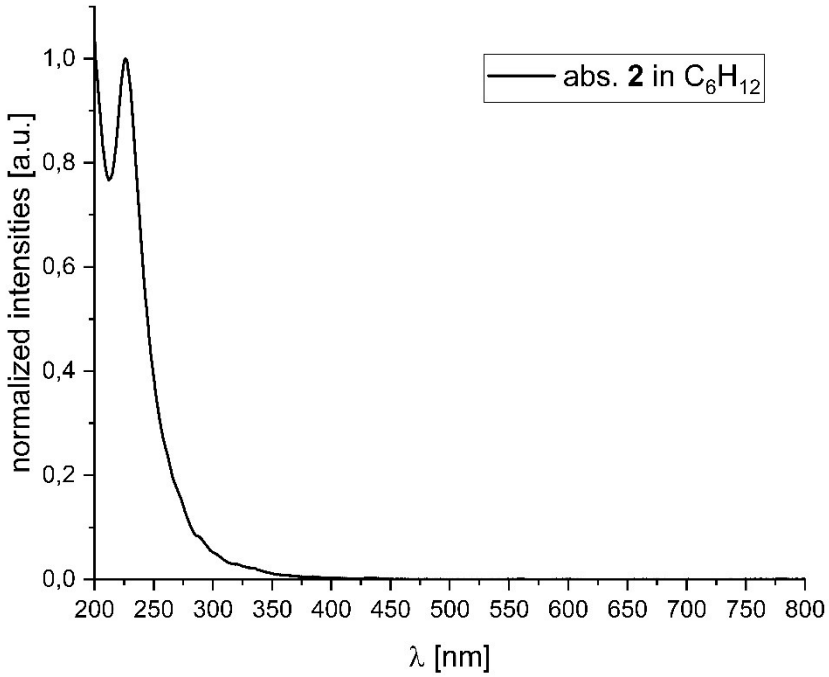

Figure S17. Normalized UV/vis absorption spectrum of **2** in cyclohexane.

2. Computational details

All quantum chemical calculations were performed using the Gaussian 16 package (Revision C.0.1).[S3] Structure optimizations were carried out using the MN15[S4] functional and the def2-TZVP basis set[S5] as implemented in Gaussian 16. To characterize the optimized structures as local minima, frequency computations were performed (no imaginary frequencies). The absolute SCF energies E^{el} of isolated molecules and the Gibbs free enthalpies G^{298} at 298.15 K and 0.101 MPa calculated at this level are given in Table S2 along with relevant relative energies.

TD-DFT calculations combined with the polarizable continuum model (PCM)[S6] calculations were performed on the optimized ground-state structures using the M062X[S7] functional and the 6-311+G(d,p) basis set, as implemented in Gaussian 16 (TD-M062X/6-311+G(d,p)//MN15/def2-TZVP). This level of theory has previously been shown to provide UV-transition energies for oligosilanes that are close to experimental values.[S8] The first 30 states were included in the TD computations (Nstates = 30).

The determination of ^{29}Si NMR chemical shieldings (σ) for the optimized structures was carried out using the GIAO method, the M06L[S9] functional, and the 6-311G(2d,p) basis set, as implemented in Gaussian 16. To minimize systematic computational errors, a benchmark set containing 14 literature-known oligosilanes was used to test the method (see Table S4). For Si atoms that are magnetically equivalent in the experimental NMR spectra due to rotations about single bonds, the average of the corresponding calculated NMR chemical shieldings was used in the benchmark study. The obtained NMR chemical shieldings were converted to the NMR chemical shift (δ) scale relative to tetramethylsilane ($SiMe_4$, T_d symmetry) using equation (1).

$$\delta^{29}\mathrm{Si} = \sigma\,(^{29}\mathrm{Si}_{\mathrm{SiMe4}}) - \sigma\,(^{29}\mathrm{Si}) \qquad (1)$$

Further information regarding the benchmark set and the results of the benchmark study can be found at the "^{29}Si NMR chemical shift" part of the Computational Details chapter.

2.1 Calculated Energies

Table S2. Absolute calculated energies of compounds of interest (MN15/def2TZVP). G^{298} was calculated for T = 298.15 K, p = 0.101 MPa.

Compound	E^{el} [a.u]	ΔE^{el}(rel) [kJ·mol^{-1}]	G^{298} [a.u.]	ΔG^{298}(rel) [kJ·mol^{-1}]
1	−22888.12923	0	−22887.34276	0
2	−22888.26535	−357[a]	−22887.47984	−360[a]
K	−22888.23098	−267[a]	−22887.44678	−273[a]
L	−22888.25092	−319[a]	−22887.47084	−336[a]
F	−22888.21787	−233[a]	−22887.43499	−242[a]
Me_6Si_2	−818.09097		−817.91106	
Me_6Ge_2	−4393.91698		−4393.74344	
$Me_3SiGeMe_3$	−2606.00443		−2605.82799	
$Me_3Si\cdot$ (^{2}A)	−408.98331		−408.90491	
$Me_3Ge\cdot$ (^{2}A)	−2196.90271		−2196.82702	
$H_3C\cdot$ (^{2}A)	−39.79155		−39.78019	
$Me_3GeSiMe_2\cdot$ (^{2}A)	−2566.06636		−2565.92654	
$Me_3SiGeMe_2\cdot$ (^{2}A)	−2566.08627		−2565.94625	
$[G]^+$	−22848.01403	0[b]	−22847.26925	0[b]
$[H]^+$	−22848.00803	+16[b]	−22847.26097	+22[b]
$[I]^+$	−22848.15538	-371[b]	−22847.41202	-375[b]
$[J]^+$	−22848.13327	-313[b]	−22847.38567	-307[b]
A	−5008.92828		−5008.11496	
$(Me_3GeGe)_4(GeMe_2)_6$	−30039.91282		−30039.13802	
B^{TMS}	−15736.47886		−15735.68099	

[a] calculated relative to compound **1**. [b] calculated relative to compound **$[G]^+$**,

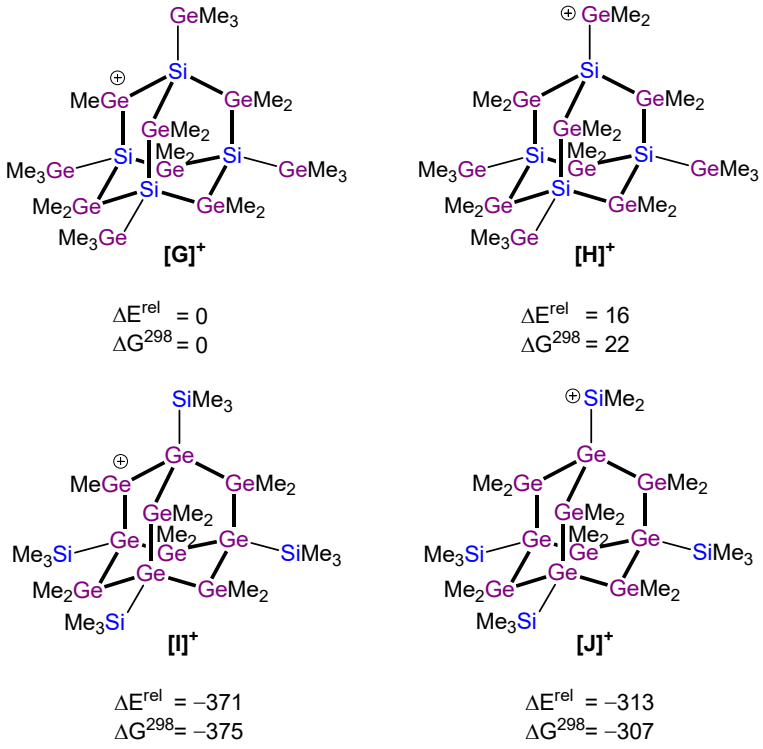

Figure S18. Comparison of relative energies ΔE^{el} and Gibbs free enthalpies ΔG^{298} in kJ·mol^{-1} of the cationic Si_xGe_y adamantanes **[G]$^+$–[J]$^+$** (MN15/def2-TZVP).

2.2 Bond dissociation energies

Table S3. Calculated bond dissociation energies (BDE^{calc}) for selected ditetrels (MN15/def2-TZVP). Experimental values (BDE^{ref}) are from references[S11,S12]

Bond	BDE^{calc} [kJ·mol^{-1}]	BDE^{ref} [kJ·mol^{-1}]
Me_3**Si–Si**Me_3	326	332(±12)
Me_3**Ge–Ge**Me_3	293	282(±15)
Me_3**Ge–Si**Me_3	311	318(±12)
Me_3GeMe_2**Si–C**H_3	385	
Me_3SiMe_2**Ge–C**H_3	332	
Me_3**Si–C**H_3		394(±8)
Me_3**Ge–C**H_3		331(±10)

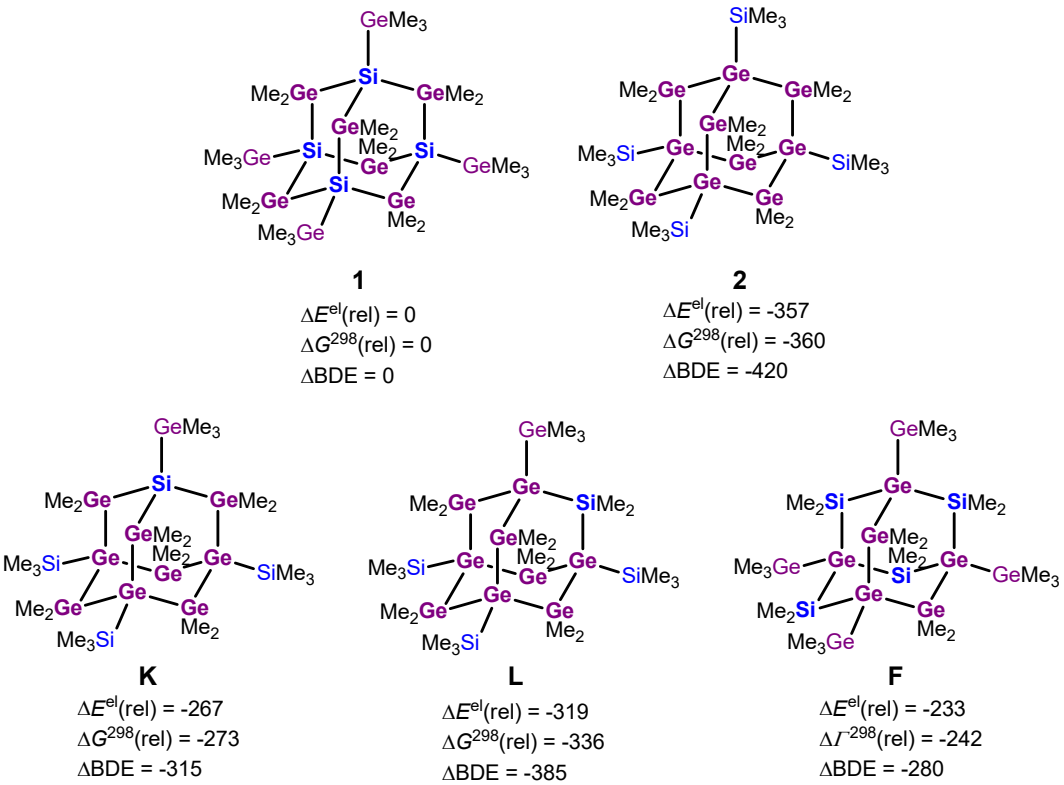

Figure S19. Calculated relative energies ΔE^{el}, Gibbs free enthalpies ΔG^{298}, and relative bond dissociation energy differences ΔBDE in kJ·mol^{-1} of the isomers **1**, **2**, **K**, **L**, **F** (MN15/def2-TZVP).

2.3 ^{29}Si NMR chemical shift values

Table S4. Absolute calculated energies of oligosilanes **T1**-**T14** used for the ^{29}Si NMR chemical shift benchmark (MN15/def2-TZVP).

#	Structure	E^{el} [a.u]	G^{298} [a.u.]
T1	$SiMe_4$	−448.92830	−448.81130
T2	Me_3SiCl	−869.22634	−869.14668
T3	Me_2SiCl_2	−1289.51930	−1289.47432
T4	$Me_3Si—SiMe_3$	−818.09098	−817.91054
T5	$ClMe_2Si—SiMe_3$	−1238.38920	−1238.24459
T6	$ClMe_2Si—SiMe_2Cl$	−1658.68633	−1658.57587
T7		−1570.39155	−1570.04661
T8	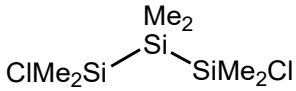	−2027.85605	−2027.67857
T9	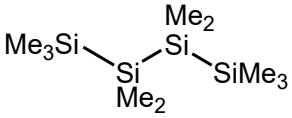	−1556.43077	−1556.11661
T10	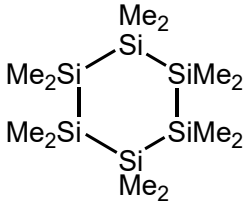	−2215.00586	−2214.62474
T11	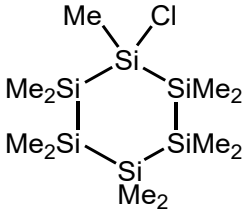	−2635.30387	−2634.95691
T12	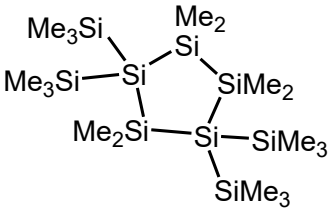	−3322.55266	−3321.95935

T13	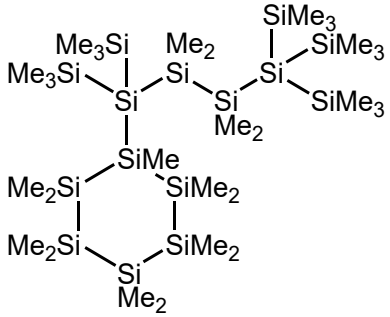	−5537.57556	−5536.56422
T14	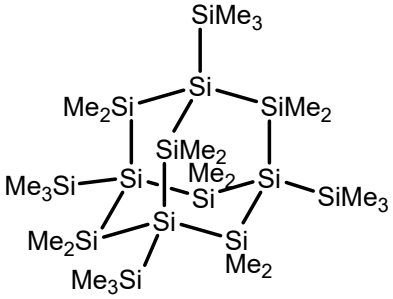	−5008.92828	−5008.11496

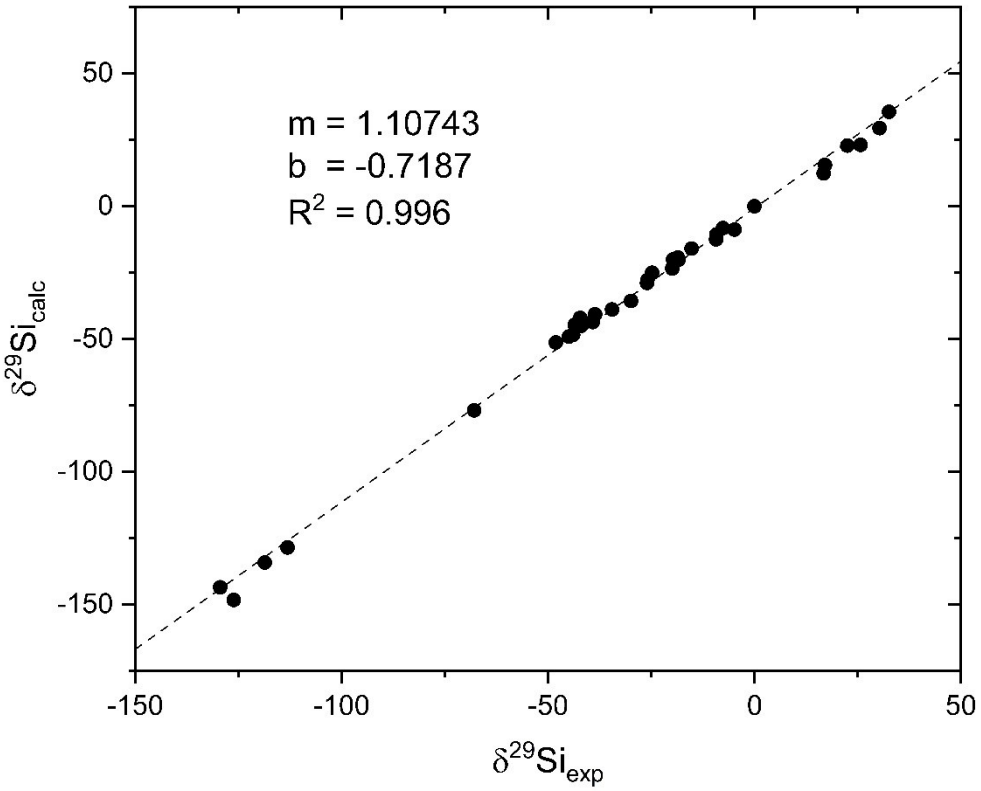

Figure S20. Correlation plot of experimental and calculated ^{29}Si NMR chemical shift values (M06L/6-311G(2d,p)//MN15/def2-TZVP) ($\delta^{29}Si_{calc} = m \cdot \delta^{29}Si_{exp} + b$).

Table S5. Calculated, linear scaled calculated, and experimental ^{29}Si NMR chemical shift values of oligosilanes **T1-T14** used for the ^{29}Si NMR chemical shift benchmark (M06L/6-311G(2d,p)//MN15/def2-TZVP).

#	Structure	NMR Calc	NMR Calc; scaled	NMR Exp.	Ref
T1	$SiMe_4$	0		0	
T2	Me_3SiCl	29.4	27.2	30.3	S12
T3	Me_2SiCl_2	35.6	32.8	32.6	S12
T4	$Me_3Si—SiMe_3$	−20.1	−17.5	−19.7	S13
T5	$ClMe_2Si—SiMe_3$	22.9 −19.3	21.3 −16.8	22.5 −18.6	S12
T6	$ClMe_2Si—SiMe_2Cl$	15.6	14.7	17.1	S12
T7	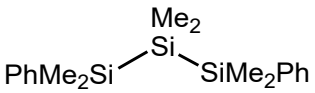	−20.1 −51.3	−17.5 −45.7	−18.4 −48.1	S14
T8	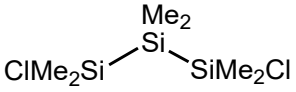	23.1 −48.4	21.5 −43.1	25.7 −43.9	S15
T9	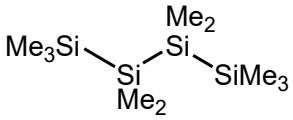	−15.9 −49.0	−13.7 −43.6	−15.2 −44.9	S13
T10	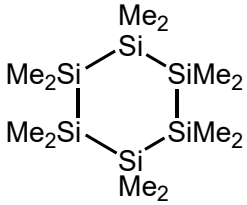	−46.1	−37.3	−42.2	S15
T11	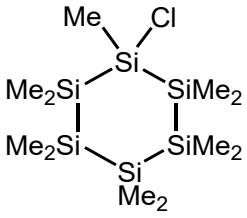	12.4 −43.6 −44.8 −49.0	11.8 −38.7 −39.8 −40.0	16.8 −39.2 −41.8 −42.1	S16
T12	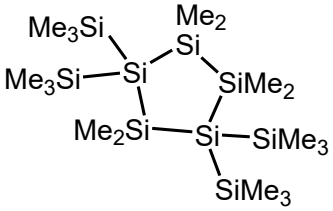	−8.2 −23.4 −25.1 −143.5	−6.7 −20.5 −22.0 −128.9	−7.6 −19.9 −24.8 −129.4	S17

T13	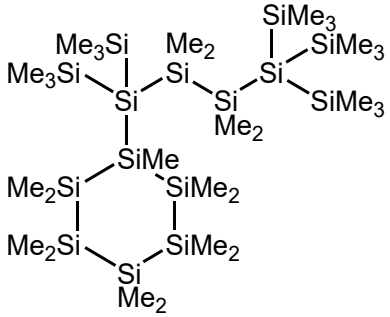	−10.6 −12.5 −27.8 −35.6 −38.8 −40.7 −44.7 −76.8 −128.5 −148.3	−8.9 −10.6 −24.5 −31.5 −34.4 −36.1 −39.7 −68.7 −115.4 −133.2	−9.2 −9.3 −25.9 −29.9 −34.5 −38.6 −43.5 −67.9 −113.1 −126.1	S18
T14	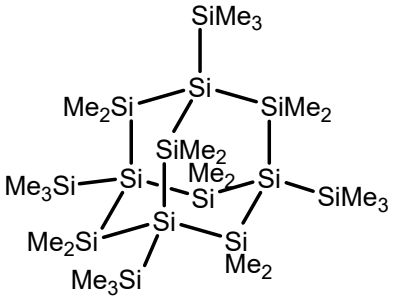	−8.8 −28.9 −134.2	−7.3 −25.4 −120.5	−4.8 −26.0 −118.6	S19

The highest impact of the linear scaling on the calculated ^{29}Si NMR chemical shifts is observed for the quaternary Si centers of the corresponding oligosilanes. The mean absolute deviation (MAD) of the unscaled ^{29}Si NMR chemical shifts of the quaternary Si atoms is MAD = 16.8 ppm compared to the scaled ^{29}Si NMR chemical shifts with an MAD = 3.0 ppm.

Table S6. Calculated and linear scaled ^{29}Si NMR chemical shift values of **1** and **2** (M06L/6-311G(2d,p)//MN15/def2-TZVP). Measured ^{29}Si NMR chemical shifts are given in parentheses.

Compound	**Calculated, scaled ^{29}Si NMR chemical shift (measured ^{29}Si NMR chemical shift)**
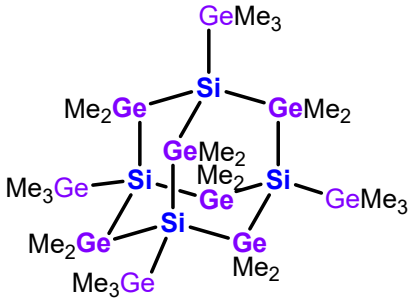 **1**	−93 (−88.8)
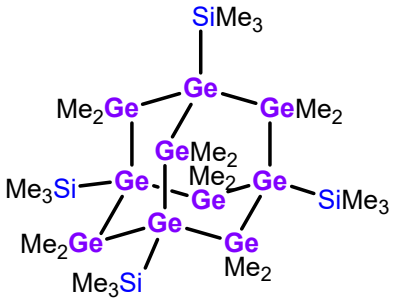 **2**	−1 (+1.4)

The calculated ^{29}Si NMR chemical shift value for the quaternary silicon atoms in **1** is overestimated by 4.2 ppm compared to the experimentally determined chemical shift value. The calculated value for the *Si*Me$_3$ atoms in **2** is underestimated by 2.4 ppm compared to the experimentally determined chemical shift value.

2.4 Calculated UV/vis spectra

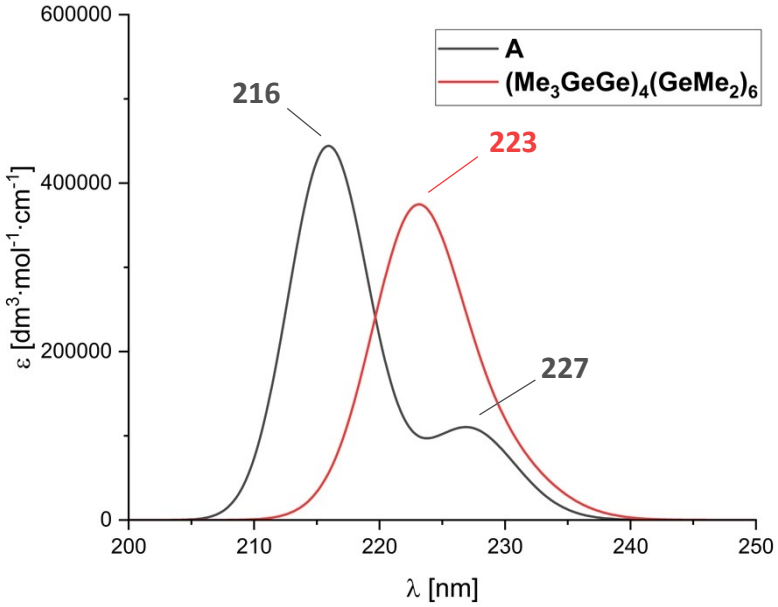

Figure S21. Calculated UV/vis spectra of **A** and the hypothetical tetrakis(trimethylgermylated) adamantane $(Me_3GeGe)_4(GeMe_2)_6$ at the PCM TD-M062X/6-311+G(d,p)/MN15/def2-TZVP level (solvent: C_6H_{12}; UV/vis band half-width at half-height = 0.1 eV = 806.5 nm).

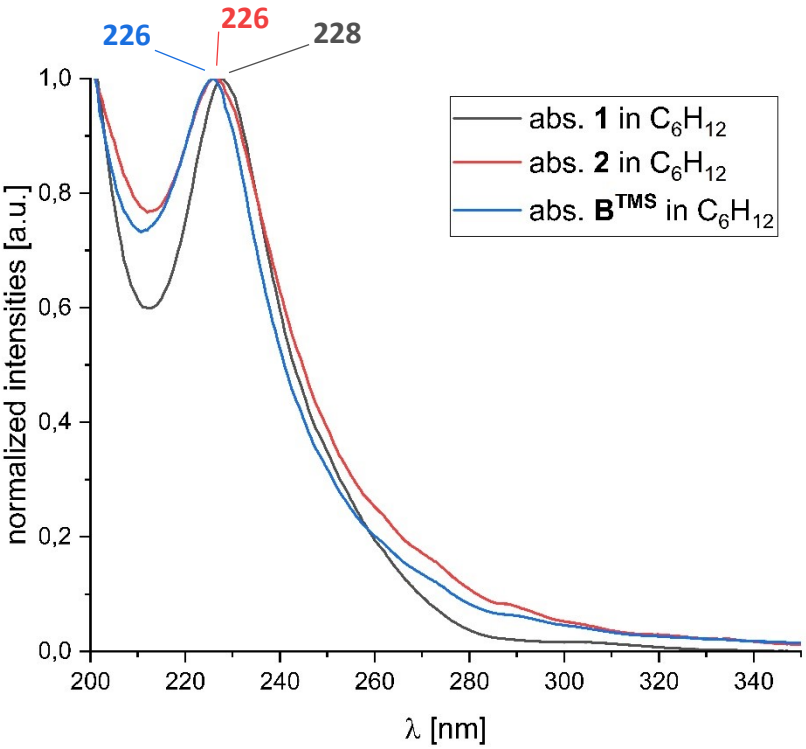

Figure S22. Experimental UV/vis spectra of compounds **1**, **2**, and $\mathbf{B}^{TMS}$ in cyclohexane.

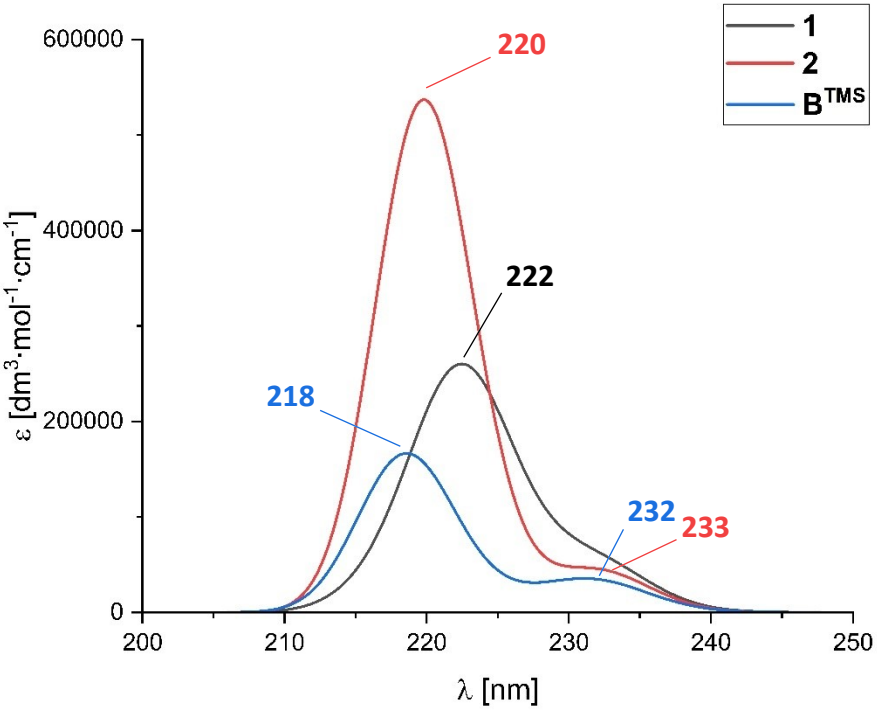

Figure S23. UV/vis spectra of compounds **1**, **2**, and $\mathbf{B}^{TMS}$, calculated at the PCM TD-M062X/6-311+G(d,p)/MN15/def2-TZVP level (solvent: cyclohexane; UV/vis band half-width at half-height = 0.1 eV = 806.5 nm).

Table S7. Singlet excitations calculated at the TD-DFT/M062X/6-311+G(d,p) level (solvent: cyclohexane).

Compound	*E* [eV]	*λ* [nm]	Oscillator strength
A	5.4646	226.89	0.2441
	5.7439	215.85	1.0510
$(Me_3GeGe)_4(GeMe_2)_6$	5.3663	231.04	0.0544
	5.4160	228.92	0.1158
	5.5458	223.56	0.5554
	5.5826	222.09	0.3384
	5.6820	218.21	0.0769
1	5.3291	232.65	0.0592
	5.3828	230.33	0.0762
	5.5426	223.69	0.1566
	5.5676	222.69	0.3643
	5.6296	220.24	0.1459
	5.7276	216.47	0.0692
2	5.3466	231.90	0.1080
	5.6178	220.70	0.7039

	5.6645	218.88	0.6746
B^{TMS}	5.3319	232.53	0.0566
	5.4061	229.34	0.0353
	5.5653	222.78	0.0251
	5.6603	219.04	0.2119
	5.6846	218.10	0.1664
	5.7357	216.16	0.0341

3. Single-crystal X-ray structure analysis of compounds 1, 2, and [K(18-c-6)][3]

Single-crystal diffraction data for **1** and **2** were collected on a *STOE IPDS II* two-circle diffractometer equipped with a *Genix 3D HS* microfocus Mo *K*α X-ray source (λ = 0.71073 Å) at 220 K (Table S8). Data finalization, including multi-scan empirical absorption corrections, was performed using the *CrysAlisPro* software version 1.171.42.43a (Rigaku Oxford Diffraction, 2022).

Single-crystal diffraction data for [K(18-c-6)][**3**] were collected at the P24 beamline of the DESY PETRA III synchrotron,[S20] equipped with a four-circle *HUBER* diffractometer with Eulerian geometry and an *X-Spectrum Lambda* 7.5M CdTe pixel array detector. The data were acquired by 360° ϕ-rotations with a 0.5° scan width using radiation of a wavelength λ = 0.500 Å (*E* = 24.797 keV).

The crystal structures were solved using the *SHELXT* program and refined against $|F|^2$ using full-matrix least-squares techniques with *SHELXL*-2018/3.[S21,S22] Further details of the structure refinement are provided in Table S8 and in the corresponding sections for each crystal structure. All H atoms were located geometrically and refined riding on the pivot atom.

Selected bond lengths in isostructural compounds **1** and **2** are given in Table S10.

CIF files containing the crystallographic information are deposited in the Cambridge Crystallographic Data Centre under the deposition codes CCDC-2545827–2545829 and can be obtained free of charge via www.ccdc.cam.ac.uk/data_request/cif. Crystallographic data, parameters of the diffraction experiments and refinement are given in Table S8.

Table S8. Crystallographic data and details of the diffraction experiments for **1**–[K(18-c-6)][**3**]

	1	**2**	[K(18-c-6)][**3**]
CCDC Deposition codes	CCDC-2545827	CCDC-2545828	CCDC-2545829
Chemical formula	$C_{24}H_{72}Ge_{10}Si_4 \cdot 0.75(C_5H_{12})$	$C_{24}H_{72}Ge_{10}Si_4 \cdot 0.75(C_5H_{12})$	$C_{33}H_{87}Ge_6KO_6Si_7$
Structural formula	$(Me_3GeSi)_4(GeMe_2)_6 \cdot 0.75(C_5H_{12})$	$(Me_3SiGe)_4(GeMe_2)_6 \cdot 0.75(C_5H_{12})$	[K(18-c-6)] $[(Me_3SiSi)_3Si(GeMe_2)_6]$
M_r	1253.18	1253.18	1251.29
Crystal system, space group	trigonal, *R*3:*H*	trigonal, *R*3:*H*	monoclinic, $P2_1/m$
Temperature (K)	220	220	100
a, ***b***, ***c*** (Å)	18.0500(4), 18.0500(4), 29.9389(11)	18.0752(4), 18.0752(4), 30.0388(9)	12.0521(3), 18.6903(3), 14.0413(3)
β (°)	90	90	112.666(3)
V (Å^3)	8447.3(5)	8499.3(4)	2918.64(11)
Z	6	6	2
***F*(000)**	3741	3741	1284
D_x (Mg m^{-3})	1.478	1.469	1.424
Radiation type	Mo Kα	Mo Kα	Synchrotron, λ = 0.500 Å
μ (mm^{-1})	5.36	5.32	1.26
Crystal color and shape	colorless plate	colorless prism	yellow-orange prism
Crystal size (mm)	0.15 × 0.14 × 0.06	0.27 × 0.17 × 0.12	0.11 × 0.07 × 0.06
T_{min}, T_{max}	0.593, 1.000	0.738, 1.000	0.799, 1.000
No. of measured, independent and observed reflections	22346, 4480, 3271 {$I > 2\sigma(I)$}	18029, 4512, 3540 {$I > 2\sigma(I)$}	26723, 5571, 4448 {$I > 2\sigma(I)$}
R_{int}	0.056	0.045	0.078
θ values (°), max, min	θ_{max} = 27.9, θ_{min} = 2.7	θ_{max} = 28.0, θ_{min} = 2.7	θ_{max} = 17.8, θ_{min} = 1.5
Range of *h*, *k*, *l*	*h* = −23→20, *k* = −22→23, *l* = −38→39	*h* = −21→23, *k* = −23→21, *l* = −39→39	*h* = -14→14, *k* = -22→22, *l* = -17→17
R*[$F^2 > 2\sigma(F^2)$], *wR*(F^2), *S	0.035, 0.110, 1.02	0.035, 0.109, 1.11	0.055, 0.143, 1.04
No. of reflections	4480	4512	5571
No. of parameters	144	143	266
No. of restraints	7	7	9
H-atom treatment	H-atom parameters	H-atom parameters	H-atom parameters

	constrained	constrained	constrained
$\Delta\rho_{max}$, $\Delta\rho_{min}$ (e Å^{-3})	0.75, −0.35	0.76, −1.12	1.44, -0.53

Computer programs: *CrysAlis PRO* 1.171.42.43a (Rigaku OD, 2022), *SHELXT* (G. M. Sheldrick, 2015), *SHELXL2019*/3 (Sheldrick, 2019), IUCr *publCIF* online service. **1** and **2**: *X-AREA* (Stoe & Cie, 2001); [K(18-c-6)][**3**]: P24 beamline local software, *CrysAlis PRO* 1.171.43.144a (Rigaku OD, 2024).

3.1 Crystal structures of the isostructural compounds 1 and 2

The crystals of the isomeric molecular compounds **1** and **2**, as well as those of the pure Si_{10} adamantane were grown from *n*-pentane (CSD refcode: **TAXPUE**; *Note*: Hereafter, six-symbol bold case CSD reference codes are given as clickable hypertext references to the Cambridge Structural Database Webpage).[S19] Their analogue with a Ge_4Si_6 cage (**VIMQUH**) was crystallized from *n*-hexane.[S23]

All these compounds are isostructural and crystallize in the trigonal crystal system with the rhombohedral Bravais lattice in the space group *R*3 (No. 148). The unit cell contains one crystallographically unique molecule, which lies on the three-fold axis (Wyckoff position *6c*) passing through one of the Me_3E–E bonds and the center of the opposite boat-like E_6 ring (E = Si or Ge, Table S9). Accordingly, the crystallographically unique part comprises six Si and Ge atoms and eight Me groups (Table S9).

Table S9. Numbering scheme for the trigonal structure type of isostructural compounds **TAXPUE**, **1**, **VIMQUH** and **2**.

	TAXPUE	**1**	**VIMQUH**	**2**	[a]
Cage	Si_{10}	Si_4Ge_6	Ge_4Si_6	Ge_{10}	
E1	**Si1**	**Ge1**	**Si04**	**Ge1**	
E2	**Si2**	**Si2**	**Ge01**	**Ge2**	
E3	**Si3**	**Ge3**	**Si03**	**Ge3**	
E4	**Si4**	**Si4**	**Ge02**	**Ge4**	
E5	**Si5**	**Ge5**	**Si06**	**Si5**	
E6	**Si6**	**Ge6**	**Si05**	**Si6**	
C1	C1	C1	C00E	C1	
C2	C2	C2	C00B	C2	
C3	C3	C3	C008	C3	
C4	C4	C4	C00A	C4	
C5	C5	C5	C00D	C5	
C6	C6	C6	C00C	C6	
C7	C7	C7	C009	C7	
C8	C8	C8	C007	C8	

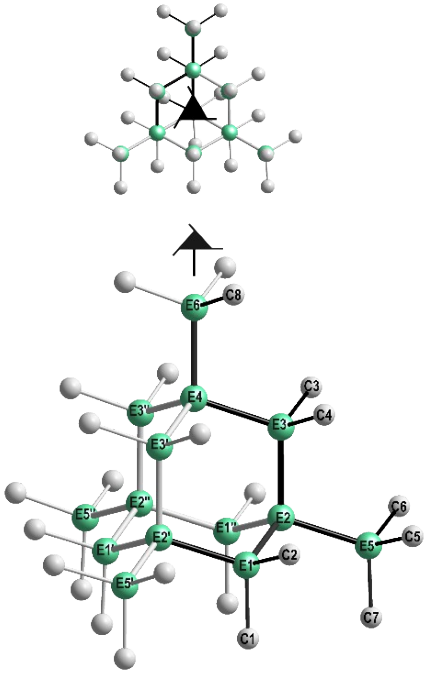

[a] Schematic representation of the labelling scheme; the color code corresponds to that in Figure S24. The crystallographic three-fold axis C_3 (▲) passes through the E4–E6 bond. The symmetrically unique bonds are shown as black lines.

The *n*-pentane solvent molecule in **1** and **2** was found to be disordered about the special position on a three-fold axis (Wyckoff position *3a*). It was modelled applying multiple constraints on the C–C bond lengths and the C–C–C angles. Note that in the crystal structures of the previously reported isotypic compounds **TAXPUE** and **VIMQUH**, the solvent molecules were not located.[S19,23]

All atomic positions of the respective cage are fully occupied only by one specific element, either Si or Ge. A model with a statistical Si/Ge distribution at each site was tested during the structure refinement; however, it resulted in poorer quality factors than the ordered model. Therefore, the molecules of **1** and **2** represent structural (positional) isomers that can be described in a simplified way as T2-supertetrahedra formed by four vertex-sharing tetrahedra.[S24] In one positional isomer (**1**), all vertices of four joined tetrahedra are occupied by Ge atoms, and all four tetrahedra are Si-centered. In the other isomer (**2**), all vertices of the T2-supertetrahedron are occupied by Si atoms, and all four tetrahedra are Ge-centered (Figure S24).

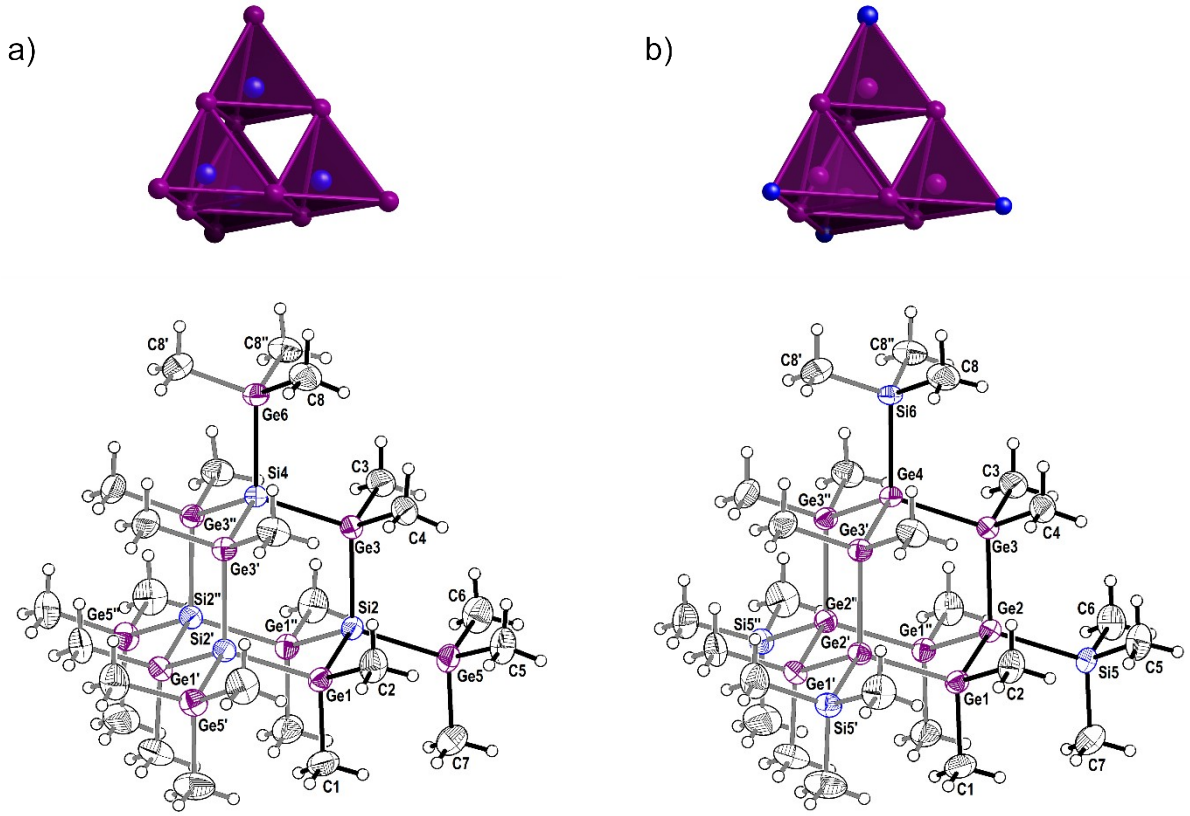

Figure S24. Molecular structures of the positional isomers (a) **1** and (b) **2** shown in polyhedral (top) and ORTEP representations (bottom; atomic displacement ellipsoids are drawn at the 50% probability level. Color code: blue: Si, purple: Ge, white hatched: C, white: H. The bonds belonging to the unique part are shown in black).

To facilitate the comparison of the geometric parameters in this series of isostructural compounds, the numbering scheme used for both **1** and **2** was adopted from the structure of the Si_{10} adamantane **TAXPUE** (Table S9). Accordingly, the corresponding positions in the E_{10} adamantane cages (E = Si, Ge) are numbered irrespective of the type of atom E, allowing direct comparison of the corresponding parameters. The bond lengths in these crystal structures are given in Table S10.

Table S10. Crystallographically unique bond lengths (Å) in the Si_xGe_y adamantanes of the trigonal structure type.

TAXPUE		**1**		**VIMQUH**		**2**	
Si_{10}		*Si_4Ge_6*		*Ge_4Si_6*		*Ge_{10}*	
Si1–Si2	2.3545(7)	Ge1–Si2	2.3939(9)	Si04–Ge01	2.3862(11)	Ge1–Ge2	2.4335(5)
Si1–Si2[a]	2.3548(7)	Ge1–Si2[a]	2.3955(9)	Si04–Ge01[a]	2.3908(11)	Ge1–Ge2[a]	2.4335(4)
Si2–Si3	2.3537(8)	Si2–Ge3	2.3909(10)	Ge01–Si03	2.3859(12)	Ge2–Ge3	2.4316(5)
Si3–Si4	2.3532(6)	Ge3–Si4	2.3935(6)	Si03–Ge02	2.3872(11)	Ge3–Ge4	2.4316(4)
Average[b]	2.3541[7]	*Average*[b]	2.3935[19]	*Average*[b]	2.388[2]	*Average*[b]	2.4326[11]
Me_3E–E							
Si2–Si5	2.3635(7)	Si2–Ge5	2.4006(8)	Ge01–Si06	2.3922(12)	Ge2–Si5	2.3968(9)
Si4–Si6	2.3590(11)	Si4–Ge6	2.3954(16)	Ge02–Si05	2.393(2)	Ge4–Si6	2.3923(15)
Average[b]	2.362[2]	*Average*[b]	2.399[3]	*Average*[b]	2.3924[4]	*Average*[b]	2.396[2]
E–Me							
Si1–C1	1.8951(18)	Ge1–C1	1.966(4)	Si04–C00E	1.889(4)	Ge1–C1	1.975(4)
Si1–C2	1.9035(16)	Ge1–C2	1.972(3)	Si04–C00B	1.882(4)	Ge1–C2	1.980(4)
Si3–C3	1.8989(15)	Ge3–C3	1.969(3)	Si03–C008	1.881(4)	Ge3–C3	1.973(4)
Si3–C4	1.8999(15)	Ge3–C4	1.966(3)	Si03–C00A	1.908(4)	Ge3–C4	1.962(4)
Si5–C5	1.9005(15)	Ge5–C5	1.957(4)	Si06–C00D	1.887(5)	Si5–C5	1.872(4)
Si5–C6	1.887(16)	Ge5–C6	1.953(4)	Si06–C00C	1.881(4)	Si5–C6	1.875(4)
Si5–C7	1.8778(17)	Ge5–C7	1.950(5)	Si06–C009	1.869(5)	Si5–C7	1.868(5)
Si6–C8	1.8860(15)	Ge6–C8	1.967(4)	Si05–C007	1.865(4)	Si6–C8	1.875(4)
Average[b]	1.894[9]	*Average*[b]	1.963[8]	*Average*[b]	1.883[13]	*Average*[b]	1.973[8] (Ge) 1.873[3] (Si)

[a] The bond length corresponds to two symmetrically equivalent bonds; the atom marked by a "[a]" symbol is generated either by (−*y*+1, *x*−*y*−1, *z*) or (−*x*+*y*+2, −*x*+1, *z*) symmetry operators. [b] The value in the square brackets is the estimated standard deviation calculated over all bond lengths of a given type, including equivalents by symmetry.

As expected, the average Ge–Ge bond length within the cluster core of the Ge_{10} adamantane **2** is further increased to 2.433[1] Å compared to the average Si–Si bonds in Si_{10} adamantanes and Si–Ge bonds in the Si_xGe_y adamantanes. This fact is in good agreement with the literature values: For the parent all-germanium adamantane $Ge_{10}H_{16}$, density-functional calculations predict Ge–Ge bond lengths spanning 2.412–2.496 Å, illustrating the substantial variability of computed values and emphasizing the need for reliable experimental structural data:[S25,26]; Si–Si, Si–Ge, and Ge–Ge bond lengths of 2.32, 2.37, and 2.42 Å, respectively, can also be calculated from published molecular single-bond covalent radii for Si (1.16 Å) and Ge (1.21 Å).[S27] For cubic silicon and α-germanium, E–E bond lengths of 2.351 and 2.450 Å, respectively, have been determined by high-precision powder X-ray diffraction (PXRD) measurements.[S28,29]

3.2 Crystal structure of the monoanionic compound [K(18-c-6)][3]

Compound [K(18-c-6)][**3**] crystallizes solvent-free in the monoclinic space group $P2_1/m$ (No. 11) as an ion pair with the general formula [K(18-c-6)][$(Me_3SiSi)_3Si(GeMe_2)_6$]. The contact-ion pair [(18-c-6)K]$^+$···Si$(Me_3SiSi)_3(GeMe_2)_6^-$ lies on the mirror plane (m_y, Wyckoff position 2*e*), resulting in two formula units per unit cell (Figure S25). Despite multiple attempts to vary crystallization conditions, only tiny (<0.1 mm), weakly scattering crystals were obtained due to the low solubility of [K(18-c-6)][**3**]. For this reason, the X-ray experiment was performed at DESY Petra III synchrotron. Slight disorder of the 18-c-6 ligand was approximated with anisotropic displacement parameters (Figure S25a).

In [**3**]$^-$, the bond lengths for the tetrahedral Si sites fall within the range of 2.3893(11)–2.4069(11) Å with an average value of 2.390[7] Å. The flattened silanide vertex is characterized by bond lengths span 2.3852(13)-2.400(2) Å (av. 2.394[4] Å). Based on these data, no detectable structural effects arising from the absence of the $SiMe_3$ group on the Si–Ge bond lengths within the heteroadamantane cage are visible. The accuracy of the bond lengths within the Si_4Ge_6 adamantane cage in [**3**]$^-$ is slightly lower than that in both **FEWWAJ** and **1** (cf. Table S11). However, the Si–Ge bond lengths are similar across all three compounds.

The K$^+$ ion is significantly shifted from the idealized local C_3 axis of the Si_4Ge_6 adamantane cage, which passes through atom Si7 and the centroid of the boat-like Si1–Ge2–Si3–Ge4–Si3'–Ge2' six-membered ring (Figure S25c, d). The Si7···K1 line forms an angle of 24.42(7)° with the local C_3 axis. The Si7···K1 bond length of 3.388(2) Å is comparable with the one reported for

the disilanide contact ion pair $[(18\text{-c-}6)K]_2\cdots[Si_2(Me_3SiSi)_2(SiMe_2)_6]^{2-}$ (3.387(4) and 3.414(4) Å), **VEPKIO**[S16]). In the latter case, each K^+ cation also coordinates to a silanide center of the Si_{10}-adamantane cage and even further deviates from the corresponding local C_3 axis of the Si_{10}-adamantane cage. The χ angles calculated from the crystallographic data deposited in the Cambridge Structural Database (**VEPKIO**) amount to 20.2(1)° and 21.3(1)°.

The sum of the Ge–Si–Ge bond angles at the silanide center Si7 in $[\mathbf{3}]^-$ amounts to 304.5(2)°, which is considerably lower than the corresponding value of 324.1(2)° for the tetrahedral Si1 and Si3 centers [an average value for 1×Si1: 324.0(2)° and 2×Si3: 324.1(2)°] within the monoanion and to the value of 326.79(7)° [an average value for 3×Si2: 326.7(1)° and 1×Si4: 327.06(6)°] for the tetrahedral Si sites in **1** In the disilanide structure **VEPKIO**, the sums of the bond angles Si–Si–Si at two silanide centers Si1 and Si3 are 308.4(5)° and 306.1(4)°, respectively.

Note that the geometric characteristics in **VEPKIO** are to be analyzed with caution due to rather high quality indicators (R_1 = 0.149, wR_2 = 0.452, S = 1.59). The rather large discrepancies between one-type characteristics calculated for heavy atoms also point to the limited accuracy of the structural model or to a certain problem with the diffraction experiment: for K···Si contacts, the discrepancy amounts to 0.025 Å, and for χ angles to 1.1°, for angle (Si–Si–Si) sums to 2.3°.

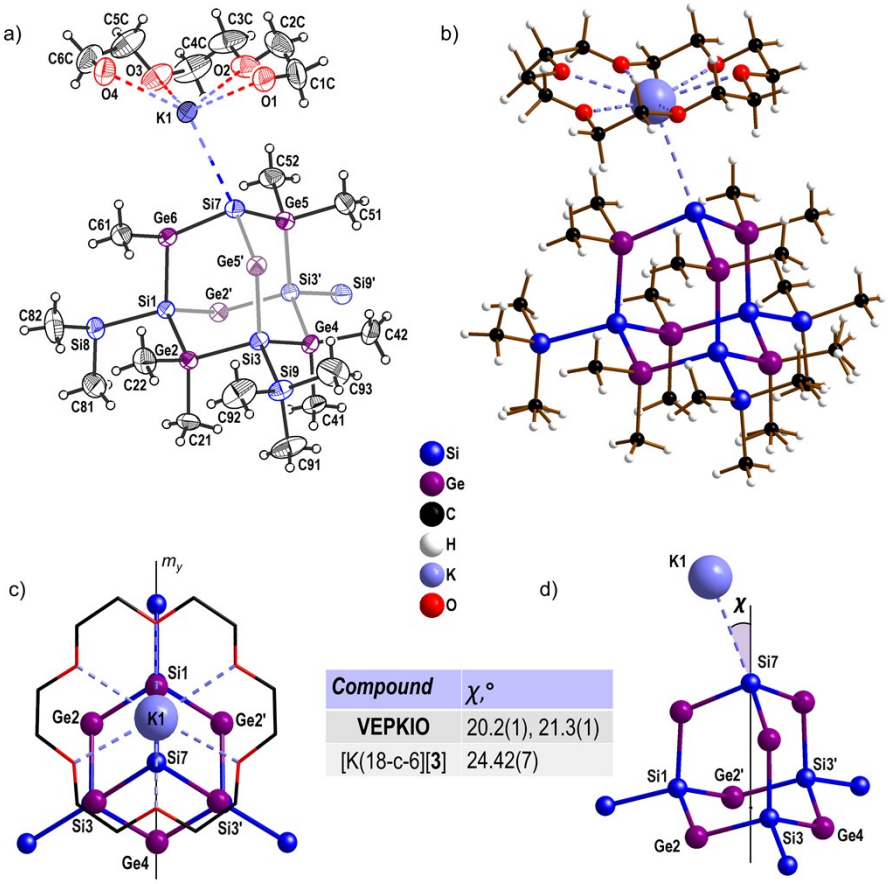

Compound	χ,°
VEPKIO	20.2(1), 21.3(1)
[K(18-c-6)][**3**]	24.42(7)

Figure S25. a) ORTEP plot of the asymmetric unit of [K(18-c-6)][**3**]. Ge and Si atoms completing the Si_4Ge_6-adamantane cage generated by the mirror plane m_y (x, 3/2−y, z) are shown in lighter color and labelled with the 'prime' symbols. Atomic displacement ellipsoids are drawn at the 50% probability level. Color code: blue: Si, purple: Ge, white hatched: C, white: H. The bonds belonging to the unique part are shown in black. b) Contact-ion pair [K(18-c-6)][**3**] in ball-and-stick representation. c) View along the local (non-crystallographic) C_3 axis of the adamantane cage, which coincides with the Si7 atom in the projection, showing the [K(18-c-6)]$^+$ cation displaced relative to this axis. The 18-c-6 ligand is shown in a wireframe model. d) Schematic definition of the χ angle, quantifying the deviation of [K(18-c-6)]$^+$ from the local C_3 axis.

3.3 Comparison of the structural characteristics in the crystallographically ordered Si_xGe_y adamantanes $(X_3SiE)_4(E'Me_2)_6$ (X = CH_3, Cl)

To date, 14 Si_xGe_y adamantanes with the general formula $(X_3SiE)_4(E'Me_2)_6$ (X = CH_3, Cl) have been structurally characterized with SCXRD. Of these, only eight crystal structures possess crystallographically ordered cages (Table S11). In all other cases, the positions of the E atoms

are shared between Si and Ge in a variable ratio, reflecting either orientational disorder of the same cage or co-crystallization of chemically different forms in one crystallographic position (CSD Refcodes for disordered Si_xGe_y adamantanes: **BIYZIW**, **BIYZUI**, and **BIZBAR**;[S30] **FEWVIQ** and **FEWVUC**;[S1] **VAKYOZ** and **VAKYUF**[S31]). Orientational disorder naturally arises from the combination of an idealized high symmetry of the rigid cage (point group T_d) and the comparable Si–Si and Si–Ge bond lengths. Isomorphous exchange between Si and Ge does not alter the size or shape of molecular cages with varying Si_xGe_y composition, allowing formation of solid solutions. Both situations are indistinguishable from the X-ray diffraction data alone due to the high symmetry of the crystal structures.

Note that splitting of the individual Si and Ge positions, although possible in principle, is often not feasible in practice because the close proximity of the cage atoms leads to strong parameter correlations and convergence problems during structure refinement, as was evidently the case for **BIYZIW**. Therefore, the mixed Si/Ge positions are refined with equated atomic coordinates for both atom types. As a result, all geometric characteristics are affected by this averaging of atomic positions. For this reason, we exclude these disordered cases from consideration.

Table S11. Bond lengths (Å) in the crystallographically ordered Si_xGe_y adamantanes $(X_3SiE)_4(E'Me_2)_6$ (X = CH_3, Cl)[a]

Cage $E_4E'_6$	Compound		E–E' (cage)			X_3E–E		Ref.
			min–max	*average*	**X = Me**	*min–max*	*average*	
Si_{10}	**TAXPUE**	Si–Si	2.3532(6)–2.3548(7)	2.3541[7]	Si–Si	2.3590(11)–2.3635(7)	2.362[2]	S19
	TAXQAL	Si–Si	2.3470(15)–2.3566(15)	2.352[3]	Si–Si	2.3641(15)–2.3777(14)	2.368[6]	S19, ESI
	VEPKIO[a]	Si–Si	2.326(5)–2.363(4)	2.345[14]	Si–Si	2.331(4)–2.359(12)	2.349[16]	S16
Si_4Ge_6	**FEWWAJ**	Si–Ge	2.3899(11)–2.3948(7)	2.3921[19]	Si–Si	2.3561(15)–2.3573(15)	2.3567[7]	S1
	1	Si–Ge	2.3935(6)–2.3955(9)	2.3935[19]	Ge–Si	2.3954(16)–2.4006(8)	2.399[3]	[b]
	[K(18-c-6)][**3**][a]	Si–Ge	2.3852(13)–2.4069(13)	2.394[7]	Si–Si	2.348(3)–2.3520(18)	2.350[2]	[b]
Ge_4Si_6	**BIYZOC**	Ge–Si	2.3812(5)–2.3892(5)	2.385[2]	Si–Ge	2.3956(5)–2.4063(5)	2.399[5]	S30
	VIMQUH	Ge–Si	2.3859(12)–2.3908(11)	2.388[2]	Si–Ge	2.3922(12)–2.393(2)	2.3924[4]	S23
Ge_{10}	**2**	Ge–Ge	2.4316(5)–2.4335(5)	2.4326[11]	Si–Ge	2.3923(15)–2.3968(9)	2.396[2]	[b]
Cage	**Compound**		**E–E' (cage)**		**X = Cl**			**Ref.**
Si_4Ge_6	**VAKYIT**	Si–Ge	2.3915(13)–2.3993(13)	2.395[2]	Si–Si	2.3139(16)–2.3226(16)	2.319[4]	S31

[a] The bond lengths for two anionic forms are listed for comparison: **VEPKIO**: $[(Me_3SiSi)_2Si_2(SiMe_2)_6]^{2-}$; [**3**]$^-$: $(Me_3SiSi)_3Si(GeMe_2)_6]^-$. [b] This work.

Comparative analysis of the ordered Si_xGe_y cages shows that the E–E' bonds are very similar for compounds with the same core, irrespective of the nature of the terminal groups (*cf*. Cl_3Si-

and Me_3Si-substituted Si_4Ge_6 cages, Table S11). This observation is consistent with the rigid geometry of this structural unit. As expected, the average E–E' bond lengths steadily increase in the series Si–Si < Ge–Si < Ge–Ge as follows: from 2.35 Å in Si_{10} to 2.39 Å in both Si_4Ge_6 and Ge_4Si_6, and to 2.43 Å in Ge_{10}. The Cl_3Si–Si bonds are significantly shorter than the Me_3Si–Si bonds (Table S11). The average Me_3E–E' bond lengths follow the same tendency, increasing by ≈0.03–0.04 Å in the order Si–Si < Ge–Si < Ge–Ge.

4. References

S1 B. Köstler, J. Gilmer, M. Bolte, A. Virovets, H.-W. Lerner, P. Albert, F. Fantuzzi and M. Wagner, *Chem. Commun.*, 2023, **59**, 2295–2298.

S2 G. R. Fulmer, A. J. M. Miller, N. H. Sherden, H. E. Gottlieb, A. Nudelman, B. M. Stoltz, J. E. Bercaw, K. I. Goldberg, R. Gan and H. Apiezon, *Organometallics*, 2010, **29**, 2176–2179.

S3 M. J. Frisch, G. W. Trucks, H. B. Schlegel, G. E. Scuseria, M. A. Robb, J. R. Cheeseman, G. Scalmani, V. Barone, G. A. Petersson, H. Nakatsuji, X. Li, M. Caricato, A. V. Marenich, J. Bloino, B. G. Janesko, R. Gomperts, B. Mennucci, H. . Hratchian, J. . Oritz, A. F. Izmaylov, J. L. Sonnenberg, D. Williams-Young, F. Lipparini, F. Ding, F. Egidi, J. Goings, B. Peng, A. Petrone, T. Henderson, D. Ranasinghe, V. G. Zakrzewski, J. Gao, N. Rega, G. Zheng, W. Liang, M. Hada, M. Ehara, K. Toyota, R. Fukuda, J. Hasegawa, M. Ishida, T. Nakajima, Y. Honda, O. Kitao, H. Nakai, T. Vreven, K. Throssell, J. E. Montgomery, J. A., Jr. Peralta, F. Ogliaro, M. J. Bearpark, J. J. Heyd, E. N. Brothers, K. N. Kudin, V. N. Staroverov, T. A. Keith, R. Kobayashi, J. Normand, K. Raghavachari, A. P. Rendell, J. C. Burant, S. S. Iyengar, J. Tomasi, M. Cossi, J. M. Millam, M. Klene, C. Adamo, R. Cammi, J. W. Ochterski, R. L. Martin, K. Morokuma, O. Farkas, J. B. Foresman and D. J. Fox, *Gaussian, Inc.*, 2019.

S4 H. S. Yu, X. He, S. L. Li and D. G. Truhlar, *Chem. Sci.*, 2016, **7**, 5032–5051.

S5 F. Weigend and R. Ahlrichs, *Phys. Chem. Chem. Phys.*, 2005, **7**, 3297–3305.

S6 J. Tomasi, B. Mennucci and R. Cammi, *Chem. Rev.*, 2005, **105**, 2999–3093.

S7 Y. Zhao and D. G. Truhlar, *Theor. Chem. Acc.*, 2008, **120**, 215–241.

S8 A. Pöcheim, G. A. Özpınar, T. Müller, J. Baumgartner and C. Marschner, *Chem. – Eur. J.*, 2020, **26**, 17252–17260.

S9 Y. Zhao and D. G. Truhlar, *J. Phys. Chem. A.*, 2008, **112**, 6794–6799.

S10 R. Becerra and R. Walsh, *Phys. Chem. Chem. Phys.*, 2019, **21**, 988–1008.

S11 Y. Apeloig, *The chemistry of organic silicon compounds Volume 2*, John Wiley and Sons Inc, Chichester, 1998, vol. 2.

S12 A. G. Sturm, T. Santowski, T. Felder, K. M. Lewis, M. C. Holthausen and N. Auner, *Organometallics*, 2022, **41**, 1960–1967.

S13 M. Ishikawa, J. Iyoda, H. Ikeda, K. Kotake, T. Hashimoto and M. Kumada, *J. Am. Chem. Soc.*, 1981, **103**, 4845–4850.

S14 R. S. Klausen, J. R. Widawsky, M. L. Steigerwald, L. Venkataraman and C. Nuckolls, *J. Am. Chem. Soc.*, 2012, **134**, 4541–4544.

S15 W. Guan, L. Lu, Q. Jiang, A. F. Gittens, Y. Wang, L. F. T. Novaes, R. S. Klausen and S. Lin, *Angew. Chem., Int. Ed.*, 2023, **62**, e202303592.

S16 T. C. Siu, M. Imex Aguirre Cardenas, J. Seo, K. Boctor, M. G. Shimono, I. T. Tran, V. Carta

and T. A. Su, *Angew. Chem., Int. Ed.*, 2022, **61**, e202206877.

S17 R. Fischer, D. Frank, W. Gaderbauer, C. Kayser, C. Mechtler, J. Baumgartner and C. Marschner, *Organometallics*, 2003, **22**, 3723–3731.

S18 A. Wallner, J. Hlina, T. Konopa, H. Wagner, J. Baumgartner and C. Marschner, *Organometallics*, 2010, **29**, 2660–2675.

S19 J. Fischer, J. Baumgartner and C. Marschner, *Science*, 2005, **310**, 825–825.

S20 "Petra III Beamline P24 EH2," can be found under https://photon-science.desy.de/facilities/petra_iii/beamlines/p24_chemical_crystallography/eh2/index_eng.html, **n.d.**

S21 G. M. Sheldrick, *Acta Cryst.*, 2008, **A64**, 112–122.

S22 G. M. Sheldrick, *Acta Cryst.*, 2015, **C71**, 3–8.

S23 S. Kühn, B. Köstler, C. True, L. Albers, M. Wagner, T. Müller and C. Marschner, *Chem. Sci.*, 2023, **14**, 8956–8961.

S24 T. Wu, L. Wang, X. Bu, V. Chau and P. Feng, *J. Am. Chem. Soc.*, 2010, **132**, 10823–10831.

S25 G. Ramachandran and S. Manogaran, *J. Mol. Struct. THEOCHEM*, 2006, **766**, 125–135.

S26 F. Marsusi, K. Mirabbaszadeh and G. A. Mansoori, *Phys. E*, 2009, **41**, 1151–1156.

S27 P. Pyykkö and M. Atsumi, *Chem. – Eur. J.*, 2009, **15**, 186–197.

S28 D. M. Többens, N. Stüßer, K. Knorr, H. M. Mayer and G. Lampert, *Mater. Sci. Forum,* 2001, **378**–**381**, 288–293.

S29 A. Dopilka, A. Childs, S. Bobev and C. K. Chan, *Chem. Mater.*, 2020, **32**, 9444–9457.

S30 M. Imex Aguirre Cardenas, T. C. Siu, A. E. Pimentel, M. O. Hight, M. G. Shimono, S. Thai, V. Carta and T. A. Su, *J. Am. Chem. Soc.*, 2023, **145**, 20588–20594.

S31 B. Köstler, M. Bolte, H. W. Lerner and M. Wagner, *Chem. – Eur. J.*, 2021, **27**, 14401–14404.